USGS
science for a changing world

# Hindcast Storm Events in the Bering Sea for the St. Lawrence Island and Unalakleet Regions, Alaska

Open-File Report 2015–1193

U.S. Department of the Interior
U.S. Geological Survey

COVER

Oblique aerial photograph of Gambell, Alaska, taken from a vantage point west of town on July 13, 2013 (photograph by Nicole Kinsman, Alaska Division of Geological and Geophysical Surveys).

# Hindcast Storm Events in the Bering Sea for the St. Lawrence Island and Unalakleet Regions, Alaska

By Li H. Erikson, Robert T. McCall, Arnold van Rooijen, and Benjamin Norris

Open-File Report 2015–1193

U.S. Department of the Interior
U.S. Geological Survey

U.S. Department of the Interior
SALLY JEWELL, Secretary

U.S. Geological Survey
Suzette M. Kimball, Acting Director

U.S. Geological Survey, Reston, Virginia: 2015



Suggested citation:
Erikson, L.H., McCall, R.T., van Rooijen, A., and Norris, B., 2015, Hindcast storm events in the Bering Sea for the St. Lawrence Island and Unalakleet regions, Alaska: U.S. Geological Survey Open-File Report 2015–1193, 47 p., http://dx.doi.org/10.3133/ofr20151193.

ISSN 2331-1258 (online)

## Acknowledgments

Funding for this study was provided by the Alaska Division of Geological and Geophysical Surveys (DGGS) Coastal Hazards Program and the U.S. Geological Survey Coastal Marine Geology Program. Field data, photos, and other critical information and data were supplied by Dr. Nicole Kinsman at DGGS. We would also like to thank reviewers Sean Vitousek and Patrick Limber, who provided constructive comments and suggestions, and Karin Ohman for assisting with initial planning and scoping of the study.

# Contents



# Figures

## Tables

# Conversion Factors

International System of Units to Inch/Pound

| Multiply | by | To obtain |
|---|---|---|
| | Length | |
| centimeter (cm) | 0.3937 | inch (in) |
| meter (m) | 3.2810 | foot (ft) |
| kilometer (km) | 0.6214 | mile (mi) |
| | Rate | |
| meters/second (m/s) | 2.237 | miles per hour (mph) |
| | Pressure | |
| kilopascal (kPa) | 0.009869 | atmosphere, standard (atm) |
| kilopascal (kPa) | 0.01 | bar |
| kilopascal (kPa) | 0.2961 | inch of mercury at 60°F (in Hg) |
| kilopascal (kPa) | 20.88 | pound per square foot ($lb/ft^2$) |
| kilopascal (kPa) | 0.1450 | pound per square inch ($lb/ft^2$) |

Temperature in degrees Celsius (°C) may be converted to degrees Fahrenheit (°F) as °F=(1.8 × °C) + 32.

# Datums

Horizontal coordinate information is referenced to the North American Datum of 1983, NAD_83(2011)(epoch: 2010).

Topographic and nearshore bathymetry were provided by the Alaska Division of Geological and Geophysical Surveys. Vertical coordinate information was converted from ellipsoid to orthometric heights, referenced to the North American Vertical Datum of 1988 (NAVD88) (Geoid12A). Because of errors in the NGS GEOID12A for parts of Alaska, orthometric heights obtained using GEOID12A as opposed to local geodetic leveling may differ from true NAVD88 elevations.

The local transformations between geodetic and tidal datums used in this report are approximate and the conversion values used are presented in the table below. These values have been derived from the orthometric heights of primary tidal benchmarks (NGS OPUS shared database) and best available local tidal station datum elevations from the 1983–2001 National Tidal Datum Epoch (NOAA CO-OPS).

| Location | Tide Station | Add this to obtain approximate local mean sea level (MSL) from NAVD88 (meters) |
|---|---|---|
| Gambell and Savoonga | Northeast Cape, St. Lawrence Island (9468039) | 0.867 |
| Unalakleet | Unalakleet (9468333) | 1.420 |

All times are reported in Coordinated Universal Time UTC. The Alaska standard time (AKST) zone is AKST=Coordinate Universal Time (UTC) minus 9 hours.

# Hindcast Storm Events in the Bering Sea for the St. Lawrence Island and Unalakleet Regions, Alaska

By Li H. Erikson[1], Robert T. McCall[2], Arnold van Rooijen[2], and Benjamin Norris[1]

## Abstract

This study provides viable estimates of historical storm-induced water levels in the coastal communities of Gambell and Savoonga situated on St. Lawrence Island in the Bering Sea, as well as Unalakleet located at the head of Norton Sound on the western coast of Alaska. Gambell, Savoonga, and Unalakleet are small Native Villages that are regularly impacted by coastal storms but where little quantitative information about these storms exists. The closest continuous water-level gauge is at Nome, located more than 200 kilometers from both St. Lawrence Island and Unalakleet. In this study, storms are identified and quantified using historical atmospheric and sea-ice data and then used as boundary conditions for a suite of numerical models. The work includes storm-surge (temporary rise in water levels due to persistent strong winds and low atmospheric pressures) modeling in the Bering Strait region, as well as modeling of wave runup along specified sections of the coast in Gambell and Unalakleet. Modeled historical water levels are used to develop return periods of storm surge and storm surge plus wave runup at key locations in each community. It is anticipated that the results will fill some of the data void regarding coastal flood data in western Alaska and be used for production of coastal vulnerability maps and community planning efforts.

## Introduction

Coastal regions of Alaska are regularly affected by intense storms of ocean origin, the frequency and intensity of which are expected to increase as a result of global climate change (Terenzi and others, 2014). In particular, regions of the State in or adjacent to the Bering Sea (fig. 1) were subjected to some notable storms in recent years, such as the low-pressure system that traversed the Bering Sea and Norton Sound in early November 2011 with wind gusts as great as 26 meters per second (m/s) (Kinsman and DeRaps, 2012). Just 3 years later in 2014, Alaskans braced for another November storm that was expected to intensify into the strongest low-pressure system ever recorded in the Bering Sea, but fortunately it turned and dissipated, leaving only little damage in its trail (Hansen, 2014).

Throughout the Arctic, sea-ice freeze-up has been occurring later than in previous years. Since the 1970s, the Chukchi Sea has experienced a trend of 6.9 days/decade delay in freeze-up (Perovich and Richter-Menge, 2009). Over the same time period, total sea-ice cover in the Bering Sea has declined 26 percent per decade. Reductions in sea-ice coverage and duration have the potential to increase the frequency and magnitude of storm impacts because larger areas of open water and later freeze-up allow

[1]U.S. Geological Survey.
[2]Deltares, Delft, The Netherlands.

for greater regions of wind/sea-surface drag, changes in heat storage and release, and changes in atmospheric-ocean interactions. However, there are currently no indications of systematic increases in Arctic storminess as a result of delayed sea-ice formation (Walsh and others, 2011). Part of the difficulty in finding causal connections between storminess and sea-ice coverage is that the analyses primarily rely on reanalysis data (Döscher and others, 2014) or anecdotal evidence, making the distinction between true and apparent changes in cyclone activity unclear. Additionally, flooding has led to millions of dollars in damage, yet many coastal flood events have gone unreported (Wise and others, 1981). This impedes development of a detailed storm climatology and the task of identifying which types of storms are most problematic for a given area (Cross, 2010). Thus, quantification of historical storm-induced water levels and frequency and extent of flood events is crucial to understanding causal relations and identifying hazards. Additionally, such quantitative information is crucial for planning and adaptation efforts that aim to assess future habitat viability, reduce loss of life and property associated with coastal flooding and erosion, and provide a baseline for analysis of future trends.

The purpose of this study is to provide viable estimates of historical (hindcast) storm-induced water levels in the coastal communities of Gambell and Savoonga, on St. Lawrence Island in the Bering Sea, and Unalakleet, located at the head of Norton Sound on the western coast of Alaska (fig. 1). Gambell, Savoonga, and Unalakleet are small permanent communities that are regularly struck by coastal storms but for which little quantitative storm data exists. The closest continuous water-level gauge is at Nome, located more than 200 kilometers (km) from both St. Lawrence Island and Unalakleet. In this study, storms are identified and quantified using historical atmospheric and sea-ice data, and the storm data are then used as boundary conditions for a suite of numerical models. The work includes storm-surge (temporary rise in water levels due to persistent strong winds and low atmospheric pressures) modeling in the Bering Strait region, as well as modeling of wave runup along specified sections of the coast in Gambell and Unalakleet. Modeled historical water levels are used to develop return periods of storm surge and storm surge plus wave runup at key locations in each community. It is anticipated that the results will fill some of the data void regarding coastal flood data in western Alaska and be useful for production of coastal vulnerability maps and community planning efforts.

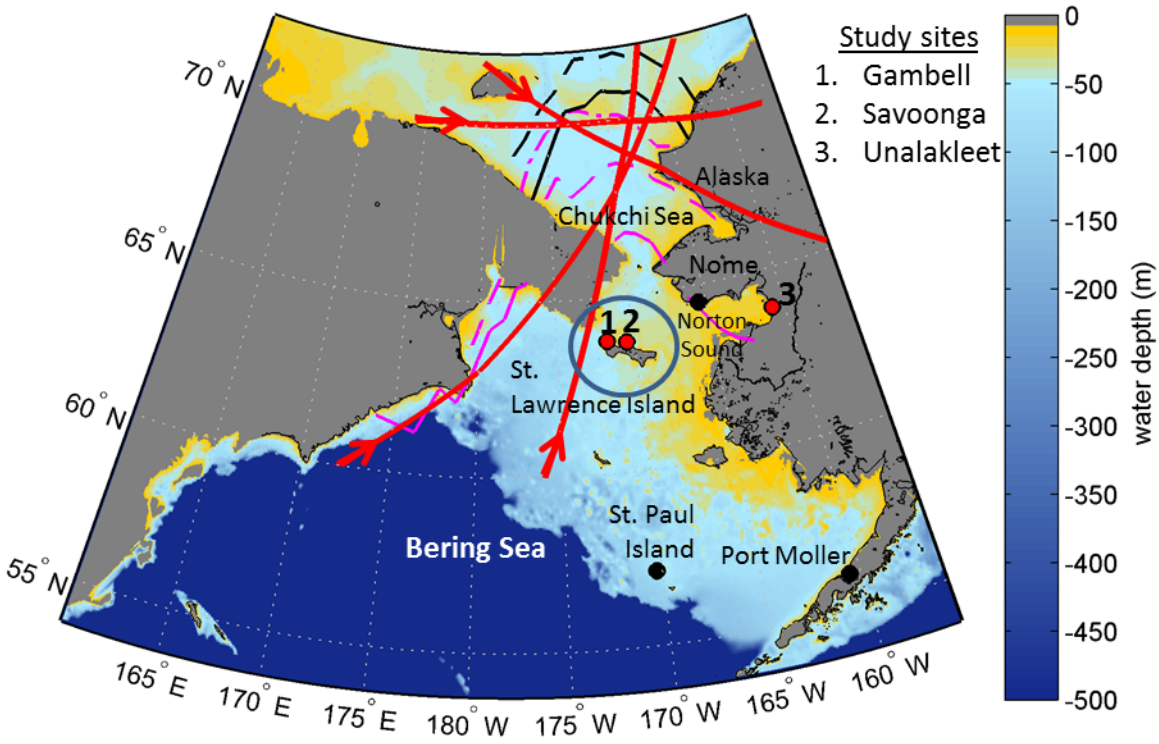


Figure 1. Map showing coastal study sites in Alaska and the surrounding region of the Bering Sea. Alaska Native villages of (1) Gambell and (2) Savoonga are located on St. Lawrence Island in the approximate center of the Bering Sea; (3) Unalakleet is located at the head of Norton Sound. Red thick lines and arrows depict typical storm tracks (Cross, 2010) that affect the study area. Waves and surges generated by storms originating in the Chukchi Sea are particularly sensitive to decreasing sea-ice extents. The northerly retreat of sea ice is exemplified with October (black lines) and November (pink lines) monthly means for three decades—1981–1990 (solid red and black lines), 1991–2000 (dashed lines), and 2001–2010 (dot-dash lines; the October extent is not shown as it is north of the map). Bathymetry data: http://www.gebco.net/data_and_products/gridded_bathymetry_data/gebco_one_minute_grid. m, meters.

## Study Sites

St. Lawrence Island lies ~250 km (~150 miles) south of the Bering Strait, ~210 km (~130 miles) southwest of Nome on the Alaskan mainland, and ~70 km (~43 miles) southwest of the Russian Chukchi Peninsula. The island is approximately 160 km long and 65 km wide at its widest point. It is believed to be one of the few remaining nonsubmerged parts of a land bridge that connected Eurasia with North America during parts of the Pleistocene until approximately 10,000 years ago (Hughes, 1984). The island is of volcanic origin with three principal areas of low mountains that reach elevations of just over 600 m. The lower slopes and lowlands are typically covered in moist tundra. Numerous ponds, lakes, and small rivers occupy approximately one-third of the surface area of the island.

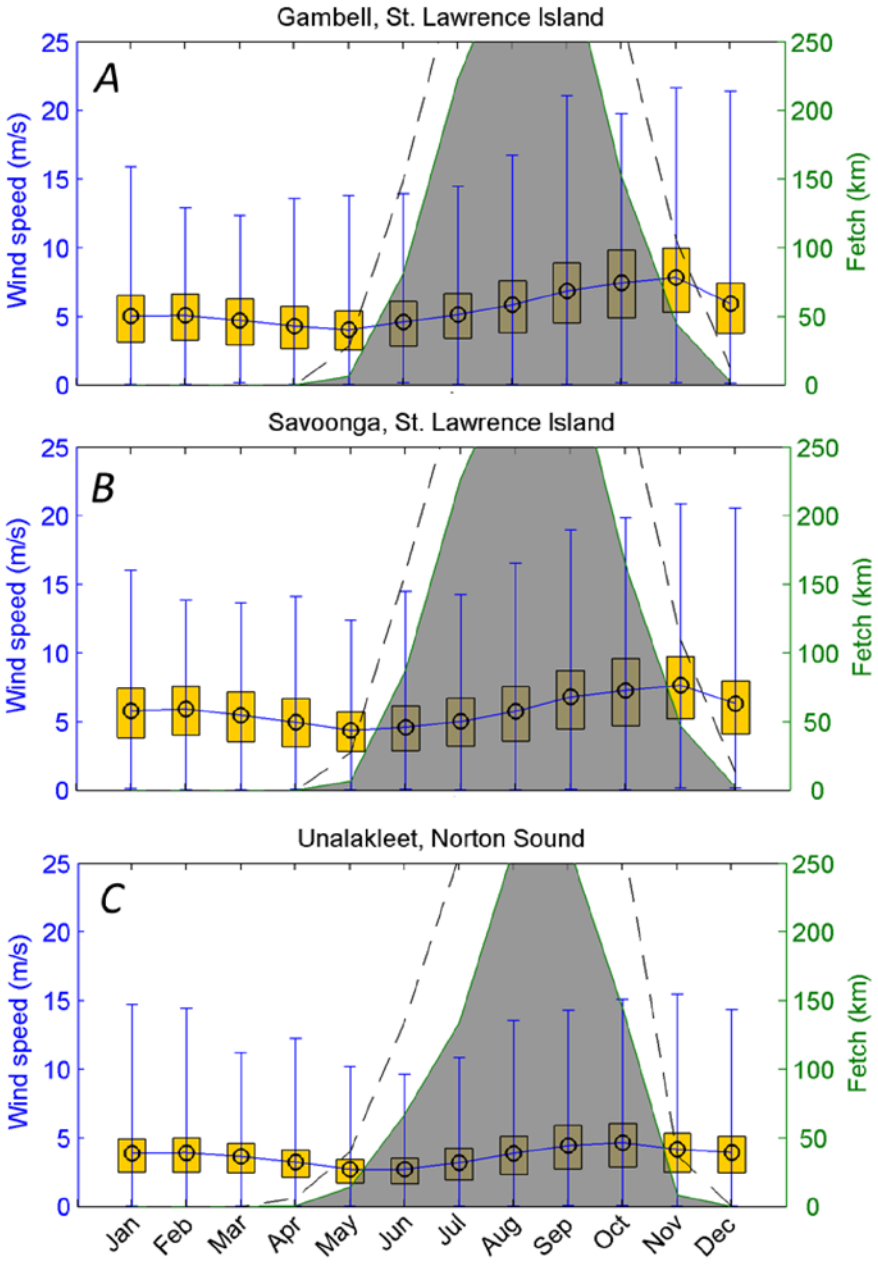


Figure 2. Graphs showing monthly windspeeds and open water fetch at each of the three Bering Sea study sites, Alaska. *A* and *B*, Gambell and Savoonga on St. Lawrence Island, respectively; *C*, Unalakleet on Norton Sound. Black circles depict mean monthly windspeeds; 25th percentile and 75th percentiles are shown with limits of yellow boxes, and maximum and minimum windspeeds are shown by the vertical lines. Gray shading and dashed lines are the monthly mean and monthly mean plus one standard deviation of the fetch and are plotted against the right-hand axis. Wind and sea-ice data were obtained from the National Oceanic and Atmospheric Administration, Earth System Research Laboratory, North American Regional Reanalysis dataset (http://www.esrl.noaa.gov/psd/data/gridded/reanalysis/) for years 1981 through 2013. m/s, meters per second; km, kilometers.

The climate at St. Lawrence Island is arctic maritime, with temperatures strongly moderated by the Bering Sea when pack ice is absent. Air temperatures are typically below freezing during the months of November through May with lowest mean monthly temperatures of about −15 degrees Celsius (°C) during January through March (based on observed data 2006 through 2014; National Climatic Data Center, NCDC, 2014). Summer temperatures are on average 8 °C and rarely exceed 13 °C. Ocean temperatures range from a couple degrees below freezing to as high as 7 °C and are modulated by annual cycles of water flow between the Pacific and Arctic Oceans across the shallow Bering Sea and through the Bering Strait (Danielson and others, 2006). Moderate to strong winds blow regularly and typically alternate between northwesterly and southwesterly directions during the summer months (June through August) and are from north-northwest during fall (September through November) at Gambell (NCDC, 2014). On the north side of the Island, Savoonga experiences west-southwest to east-northeasterly winds during the summer months and north-northwesterly winds during the fall. Average monthly windspeeds are lowest during the summer (5–8 meters per second, m/s) and greatest during the fall/winter months (~10 m/s, fig. 2). High wind events, those associated with storms, follow a similar seasonal/annual trend of lower and higher speeds during summer versus fall and winter. Windspeeds greater than 10 m/s are common during the fall and winter (75th-percentile windspeeds, fig. 2). The highest recorded windspeeds between 2006 and 2014 were 29.2 m/s and 38.9 m/s at Gambell (November 9, 2011) and Savoonga (February 27, 2009), respectively (NCDC, 2014) but may reach higher speeds as the record length of observation is quite short (less than 10 years).

High winds and frequency of storm events is of most concern when the Bering Sea and coast are free from ice. The advance and retreat of the ice pack in the Bering Sea is dominated by wind-driven advection (Overland and Pease, 1982; Danielson and others, 2006); sea ice typically reaches St. Lawrence Island in November/December and retreats to expose “open water” in May. The fetch, or distance over open water that winds blow to form waves and storm surge, is typically limited (less than 50 km) and insufficient for substantial wave growth between the months of mid-November through mid-May (fig. 2). Although this has been true historically, the greater intensity and frequency of storms during October through December has the potential to adversely impact coastal communities as the monthly mean fetch increases in response to climate change (figs.1 and 2).

The most commonly observed storm tracks that reach western Alaska and the Bering Sea originate in the North Pacific, and to a lesser degree, in the Arctic. Typical storm tracks that affect the Bering Sea were summarized by Cross (2010, fig. 2.3) and are shown with red solid lines in figure 1. North Pacific storms often begin and intensify over the warm western boundary of the Kuroshio Current east of Japan. These storms form as cold, dry air masses from Siberia meet with mild and moist subtropical air masses off the coast of Japan, where they can deepen (drop in pressure) and travel northwestward toward Alaska. The other dominant storm track entering the Bering Sea from the south is often linked to the Aleutian Low (a semi-permanent low pressure center located near the Aleutian Islands); these traveling cyclones (large areas of closed inward-spiraling winds rotating counterclockwise in the Northern Hemisphere) reach maximum intensity (low pressures) centered around the Aleutian Islands (Rodionov and others, 2007; Mesquita and others, 2010). Although less commonly affecting storm activity in the Bering Sea, cyclones that develop in the Arctic (Hume and Schalk, 1967; Lynch and others, 2003) over Siberia can move northeast to the East Siberian and Arctic Seas. On occasion, these storms are guided by upper level atmospheric steering and traverse east and south to the Bering Sea.

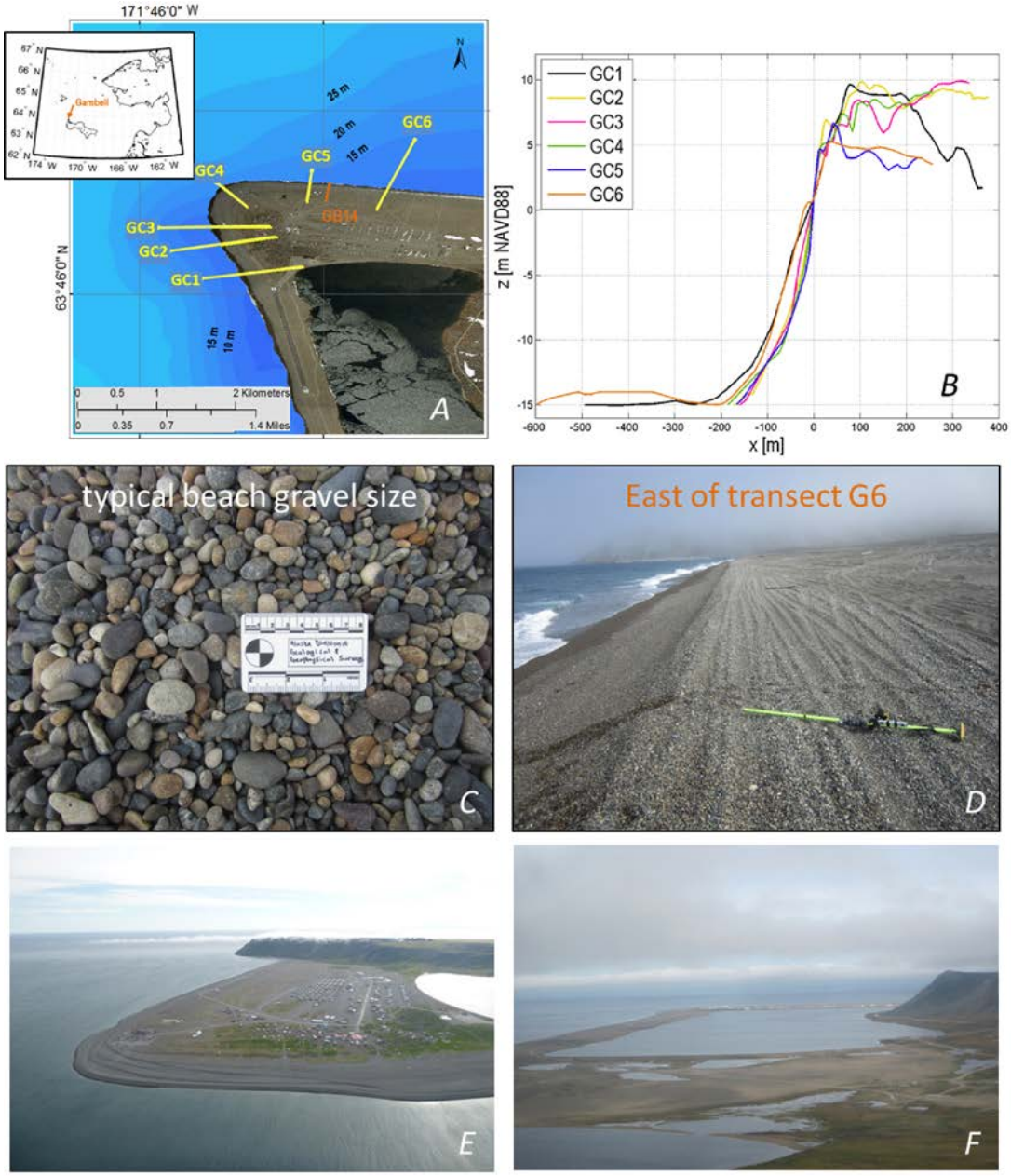


Figure 3. Map, graph, and images for the Gambell study site on St. Lawrence Island, Alaska. *A*, Map/aerial image showing that community infrastructure is primarily located along the northwest and north coasts of the tip of St. Lawrence Island, with an airstrip abutting the west coast near the center and bottom of the image. Troutman Lake appears in the southeast quadrant of the image. Storm surges were simulated for the full 1981 through 2010 time period. Wave runup was calculated for select storms at transects GC1 through GC6. (Photograph *A* courtesy of Alaska Department of Commerce, Community, and Economic Development. Bathymetry constructed from measurements obtained by Alaska Division of Geological and Geophysical Surveys.) *B*, Graph of cross-shore profiles merged from bathymetry and topography data and used in wave-runup simulations. Foreshore (beach) slopes were steep to mild on the west side (~1:10 to 1:16) and steep (1:7 to 1:10) on the north side. *C* and *D*, Photographs of beach sediments, which were primarily composed of gravels. *E* and *F*, Aerial photographs of Gambell taken in August and September 2014. (*C* through *F*, courtesy of Alaska Division of Geological and Geophysical Surveys.) m, meters; NAVD88, North American Vertical Datum of 1988.

Gambell and Savoonga are the only permanent population centers on St. Lawrence Island; these Alaska Native tribal villages received joint title to most of the land on St. Lawrence Island under the Alaska Native Claims Settlement Act of 1971. Gambell is located on a gravel bar at the island's Northwest Cape (fig. 3*A*) and hosts a population of 681 mostly (more than 95 percent) Native persons (U.S. Census Bureau , 2014). Elevation of the developed and surrounding areas that have infrastructure and archeological sites are at relatively low (~5.92±1.87 meters, m, North American Vertical Datum of 1988, NAVD88; average of approximate land area shown in fig. 3*A*). Much of the area is characterized by bare or sparsely vegetated gravel. The beaches are composed of gravel and are relatively void of vegetation (fig. 3*C*). Goods and persons are transported to and from the community either by boat or more commonly by plane. Gambell Airport, originally built in 1943, hosts a runway along the west coast of the island at ~8 m above approximate mean sea level (MSL; Federal Aviation Administration, 2014).

Westerly storms cause the greatest impacts in Gambell. As no permanent tide, water level, or wave gauges exist, flood elevations are primarily based on anecdotal evidence. Residents estimate that westerly storms have brought maximum wave heights of ~8 m (28 feet, ft); in contrast, easterly and northerly storms are estimated to yield much lower wave heights at ~3 m (10 ft) (Floodplain Manager, Gambell City Office, written commun., 2011). Waves at Northwest Cape vary in height as the larger western waves refract around the point. The September 1972 storm overtopped the beach ridge and flooded the runway with as much as 0.5 m (1.5 to 2 ft) of water. More recently, the November 2011 storm caused minor coastal flooding with waves on the order of 7 m (20 ft) and total water levels ~3 m (8–10 ft) MSL (NCDC, 2014). Other westerly storms have caused sheet flows and deposited as much as 15 cm (half a foot) of beach gravel across the runway (Floodplain Manager, Gambell City Office, written commun., 2011). Storm surges are thought to be less than 2 m (less than 6.6 ft) because of relatively good return flow conditions created by bathymetry and topography (Ostrom and others, 1987). Elevated water levels due to storm surges percolate through the coarse gravel leading to seawater pools in low-lying parts of town. The last reported significant flood event was in 1977 (Floodplain Manager, Gambell City Office, written commun., 2011).

In contrast to Gambell where storms from the west cause the greatest concern, Savoonga, located on a low broad point on the north shore of St. Lawrence Island is mostly affected by northwesterly storms (fig. 4). Similar to Gambell, Savoonga hosts a small mostly (95 percent) Native population of 671 persons (U.S. Census Bureau, 2014).

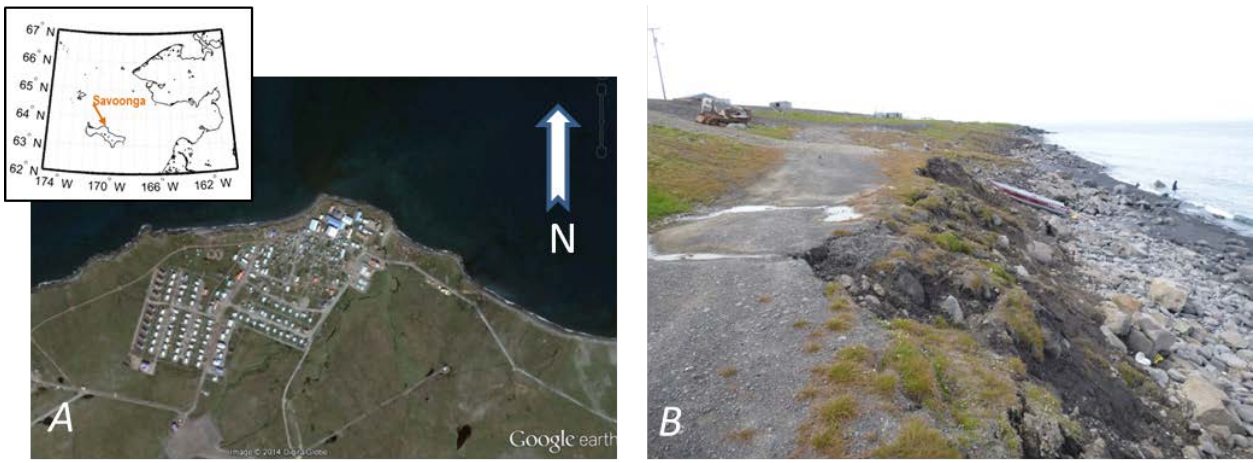


Figure 4. Photographs of the Savoonga study site on St. Lawrence Island, Alaska. *A*, Satellite image showing overview of Savoonga (Google Earth image). *B*, Erosion along north exposed shoreline (photograph taken 2014, courtesy of Alaska Division of Geological and Geophysical Surveys).

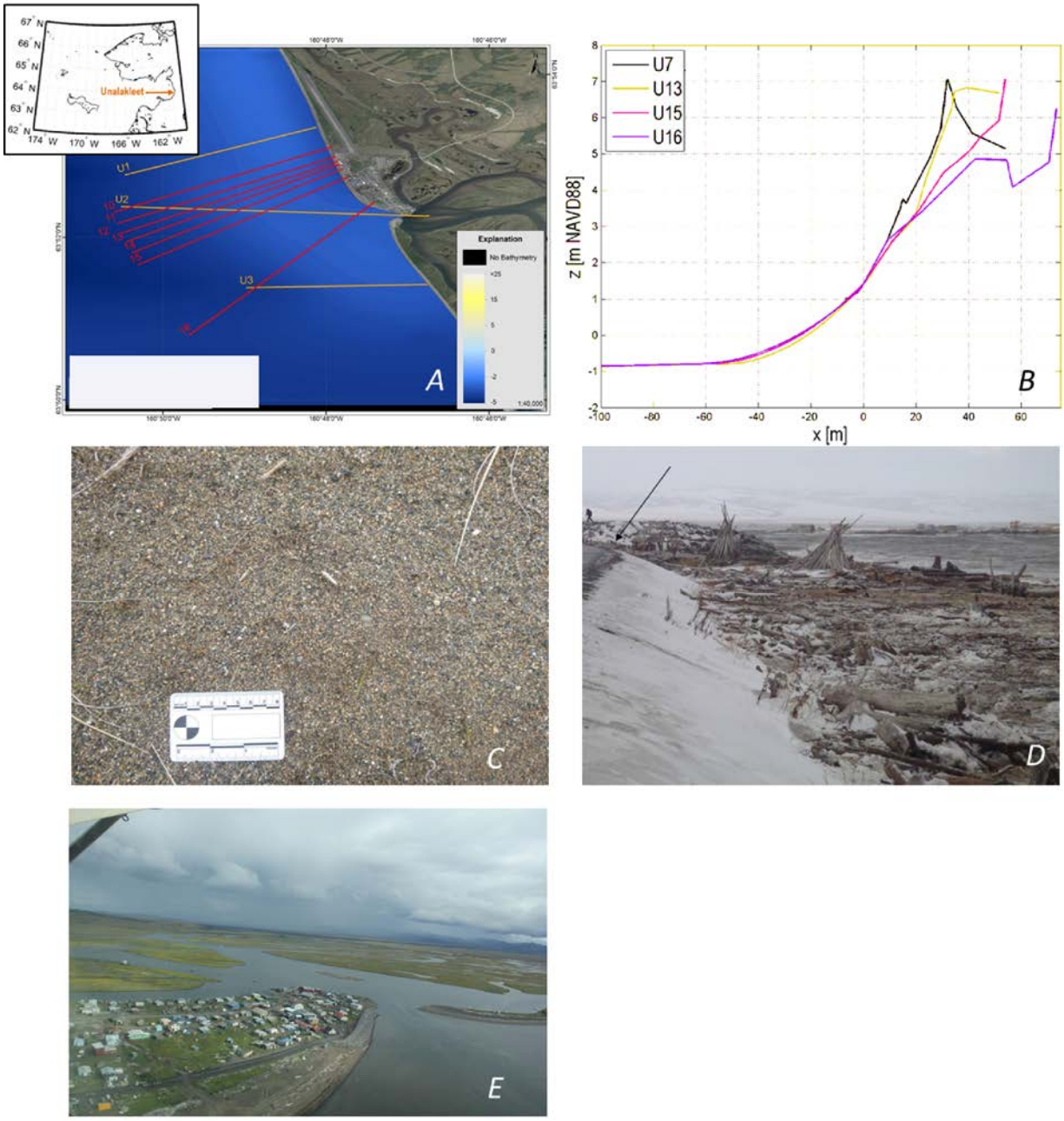


Figure 5. Map, graph, and images for the Unalakleet study site on St. Lawrence Island, Alaska. Storm surges were simulated for the full 1981 through 2010 time period. *A*, Map/aerial image showing selected storm transects for which wave runup was calculated—U7, U13, U15, and U16. Transect U7 is located about 7 kilometers north of Unalakleet and is not shown. Bathymetry is in meters. (Photograph used in *A* courtesy of TerraMetrics and Digital Globe 2015; bathymetry constructed from measurements obtained by Alaska Division of Geological and Geophysical Surveys.) *B,* Graph of cross-shore profiles merged from bathymetry and topography data and used in wave-runup simulations. *C,* Photograph showing beach sediment, which is primarily composed of medium grained sands (courtesy of Alaska Division of Geological and Geophysical Surveys). *D*, Photograph taken near transect U16 modified from Kinsman and DeRaps (2012). *E*, Aerial photograph of Unalakleet taken in 2010 (National Oceanic and Atmospheric Administration photograph by John Cloud downloaded from https://en.wikipedia.org/wiki/Unalakleet,_Alaska). m, meters; NAVD88, North American Vertical Datum of 1988.

Whereas Gambell and Savoonga are located on St. Lawrence Island in the middle of the Bering Sea, the Native Village of Unalakleet (population 688, 77 percent Alaska Natives, U.S. Census, 2010) is situated near the end of a low lying sand and gravel spit on mainland Alaska at the head of Norton Sound (fig. 5). All three sites are located at similar latitudes (63.7° N to 63.9° N) but the westerly exposure and shallow (~20 m) focused water body of Norton Sound enables relatively greater storm-surge levels to affect Unalakleet. Historical observations indicate a storm surge as high 6.1 m MSL in 1960 (Wise and others, 1981). Other extreme events include 5.5 m and 4.6 m levels in 1964 and 1974, respectively (U.S. Army Corps of Engineers, 2011). Extreme surge events along the open coast of Unalakleet were modeled by Chapman and others (2009). The ten largest surge events identified ranged from 2.8 m (9.3 ft, October 18, 1991) to 4.8 m (16.0 ft, October 1, 1960) for the simulated time-period of 1954 through 2004.

## Methods and Model Input Data

With the aim to quantitatively evaluate flood risk on St. Lawrence Island and along the open coast of Unalakleet, the contributions of tides, storm surges, and wave runup were evaluated individually and in combination. During any storm event it is the superposition of tides, surges, and wave runup that make up the total water level (TWL, fig. 6). However, the relative contribution of each varies depending on location and timing of storm events with respect to astronomic tides and, as such, one process may be more important than another for a given setting. Surge and wave runup modeled in this study were done without regard to tide stage; this approach was also taken by Chapman and others (2009) for storm-surge simulations. This was done to eliminate the task of extracting individual component water levels from a time-series of TWLs, which is required for calculation of statistical return periods. Furthermore, emulating tide-independent storm-surge levels allows for greater flexibility in evaluating realistic realizations of concurrent tide and storm-surge levels, including worst case scenarios. Nontidal currents, induced by storm-surge hydrodynamics and wave propagation are explicitly accounted for in the model, but tidal current interaction and the effect of tide stage on wave growth and decay are not. Whereas this approach slightly reduces accuracy when compared to actual storm water levels, it is speculated that the errors are small due to the low tidal amplitude (~20 to ~50 centimeters, cm) and relatively weak tidal currents (~15 centimeters per second, cm/s) near the east end of St. Lawrence Island (Danielson and Kowalik, 2005).

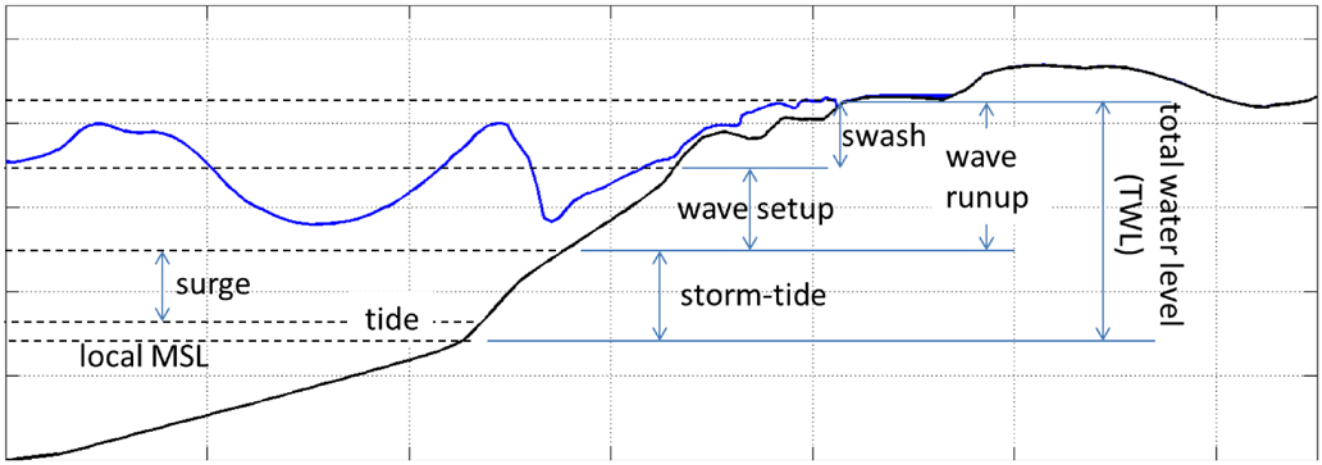


Figure 6. Definition sketch of water levels referred to in this report. Total water levels (TWL) sometimes exclude the swash (uprush and downrush of wave motion on the beach face), but in this study the swash is included in estimates of TWL.

This study involved four phases of numerical modeling. The four phases are briefly summarized below and details of the models (listed in table 1) are described in subsequent sections. All Delft3D models employed in this study are open-source (see http://oss.deltares.nl/web/delft3d).

*Astronomic tides*—The Delft3D-FLOW model was calibrated and compared against tidal variations measured at Nome, St. Paul Island, and Port Moller (fig. 1). The closest tide station to both St. Lawrence Island and Unalakleet is at Nome, located more than 200 km from each study site. Following a first-order calibration, the model was run for a 30-day period. Tidal constituent amplitudes and phases were calculated from water levels simulated at each of the three study sites. Derived constituents were initially used to estimate the astronomic tides at Gambell, Savoonga, and Unalakleet; these have since been updated with model-derived values published by NOAA (2014).

*Probability of flooding due to storm surge*—The Delft3D-FLOW model was calibrated and validated against nontidal water level variations measured at Nome, Gambell, and Unalakleet using time- and space-varying reanalysis wind and pressure fields for atmospheric forcing. Production runs for the open water season of years 1981–2012 were then performed. Statistical flood frequencies (return-value curves) were calculated from the simulated 32-year semicontinuous time-series of hourly water levels at Gambell, Savoonga, and Unalakleet. Return values were calculated using the peak-over-threshold (POT) generalized Pareto distribution (GPD), generalized extreme value (GEV), and log-linear fits.

*Probability of flooding due to storm surge plus wave runup*—Time-series data of offshore waves from already available hindcast simulations were propagated to the nearshore using the Delft University of Technology's Delft3D-WAVE (Simulating Waves Nearshore, SWAN) model. Spatially and temporally varying reanalysis wind fields were applied to the model domains to allow for local wave generation. Time-varying storm-surge levels and wave conditions (significant wave heights, SWH; mean wave directions, $D_m$); and peak period, $T_p$) for select storms were then applied at the offshore boundary of cross-shore XBEACH models (http://oss.deltares.nl/web/xbeach/) for computation of surge and wave runup at the coast. Storms were selected by first simulating wave propagation for the largest 90 surge events identified from the 32-year simulation mentioned above. Wave runup was estimated with a look-up table and added to simulated nearshore storm-surge levels. The largest 30 events of the 90 that included storm surge and estimated wave runup were selected and XBEACH models were run

using actual measured cross-shore profiles in the communities of Gambell and Unalakleet. Return values of water levels from surge and wave runup were calculated using the same approach as was done for the storm-surge levels. The overall approach is illustrated with the flow chart in figure 7.

Relative contributions of storm surge, wave runup, and tides to the TWL were calculated and evaluated for Gambell and Unalakleet.

Table 1. Summary of processes simulated and numerical models employed at each of the three Bering Sea study sites, Alaska.

| Study site | Storm-surge levels (Delft3D-FLOW model) | Wave propagation (Delft3D-WAVE, Simulating Waves Nearshore ,SWAN, model) | Wave runup (XBEACH model) |
|---|---|---|---|
| Gambell | **x** | **x** | **x** |
| Savoonga | **x** | | |
| Unalakleet | **x** | **x** | **x** |

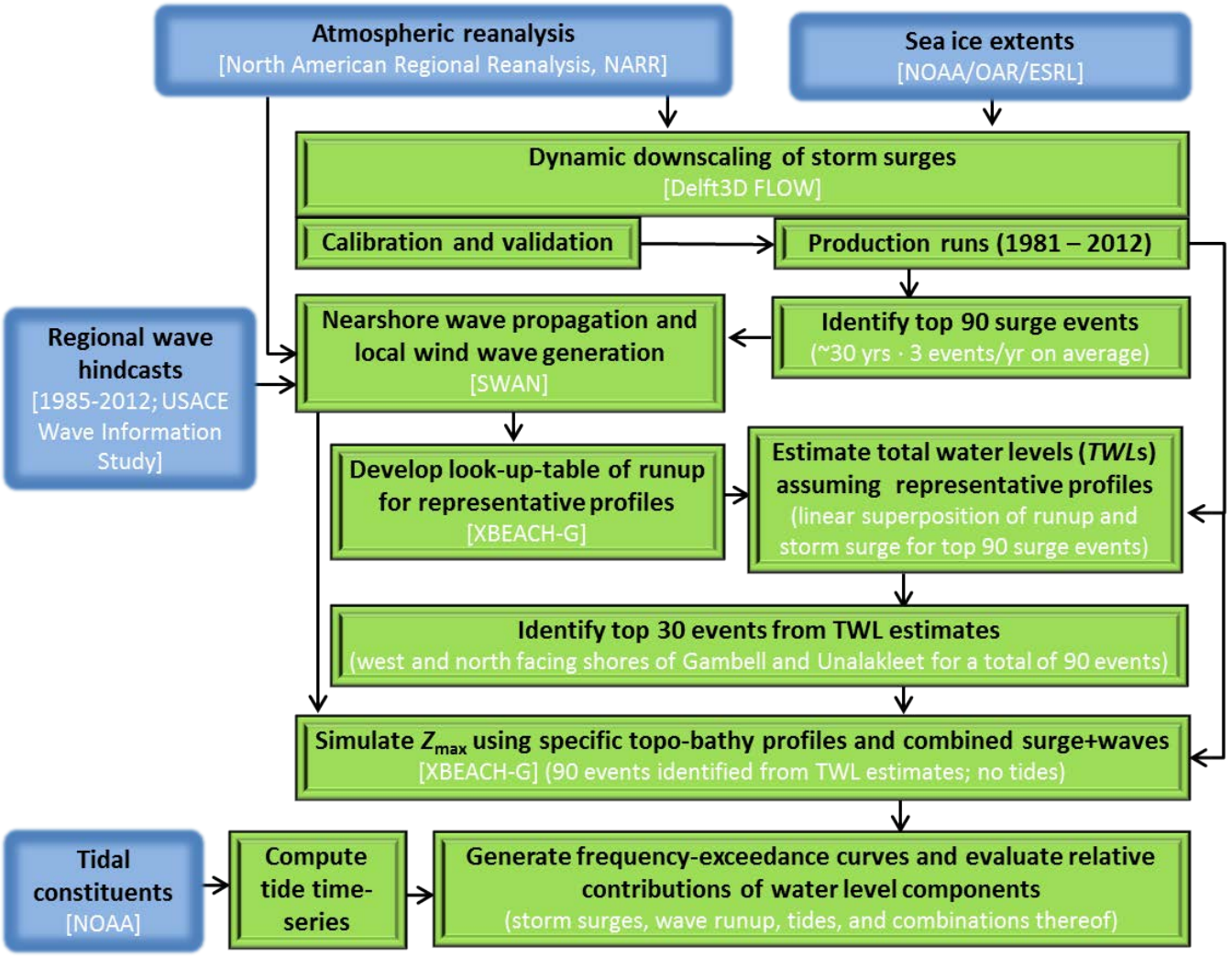


Figure 7. Flow chart illustrating the approach employed to estimate flood-level exceedances of modeled storm surge and wave runup. Green boxes refer to tasks undertaken as part of this study and blue boxes represent external data used as inputs and boundary conditions in the models. Delft3D and XBEACH models employed in this study are open-source (see http://oss.deltares.nl/web/delft3d and http://oss.deltares.nl/web/xbeach/). NOAA, National Oceanic and Atmospheric Administration; NOAA/OAR/ESRL, NOAA, Oceanic and Atmospheric Research, Earth System Research Laboratory; USACE, U.S. Army Corps of Engineers; TWL, total water levels (TWL); yr, year.

## Tide and Storm Surge Model

Water level variations associated with tides and storm surge were calculated with the Deltares Delft3D-FLOW (ver. 4.00.01) model (Lesser and others, 2004; Deltares, 2011). Delft3D is an integrated modeling suite that has the ability to model three-dimensional flow although all simulations done for this study were accomplished in a depth-averaged mode. The Delft3D-FLOW module solves the Navier-Stokes shallow water equations and is comparable to the ADCIRC model used by Chapman and others (2009).

The hydrodynamic model consists of several two-way coupled grids of varying resolution (fig. 8). The model domain stretches from the Russian Siberian coast to Alaska's west coast and extends

from the southern end of the Aleutian Islands (53.8° N) to 72.0° N, in the Chukchi Sea. Grid resolution ranged from 5 km in the northern and southern extents of the domain to 100 m at the study sites. The 100-m parts of the grid were later redefined to 500-m resolution after a sensitivity analyses showed little difference in water levels with the finer grid. This reduced computation time five-fold so that approximately 1 hour of computation time yielded 2 days of simulated time. Tidal variations were driven by astronomic constituents applied at the open boundaries in the Chukchi and lower Beaufort Seas. A total of 13 tidal constituent amplitudes and phases ($M_2$, $S_2$, $N_2$, $K_2$, $K_1$, $O_1$, $P_1$, $Q_1$, $M_F$, $M_M$, $M_4$, $MS_4$, and $MN_4$) were applied at the open boundaries with initial estimates obtained from the TOPEX7.2 global tide model (Egbert and Erofeeva, 2002). Bathymetry was compiled from three sources (table 2). Data obtained by Alaska Division of Geological and Geophysical Surveys (DGGS) in the nearshore shallow waters of Gambell and Unalakleet were linearly interpolated in the alongshore direction across the near-normal cross-shore bathymetry data lines. Nearshore regions in the vicinity of the study sites where data has not been recently collected were populated with NOAA soundings from 1968 and 1970. These data are old but, considering the horizontal resolution, are a better representation of nearshore depth variations compared to the more coarse-gridded data products available. Remaining areas away from the immediate vicinity of the three study sites were populated with the GEBCO08 global 1-arc minute bathymetric dataset (http://www.gebco.net/data_and_products/gridded_bathymetry_data/gebco_one_minute_grid/). All data were converted to MSL and interpolated in regions of data overlap to provide smooth transitions between the various data sources.

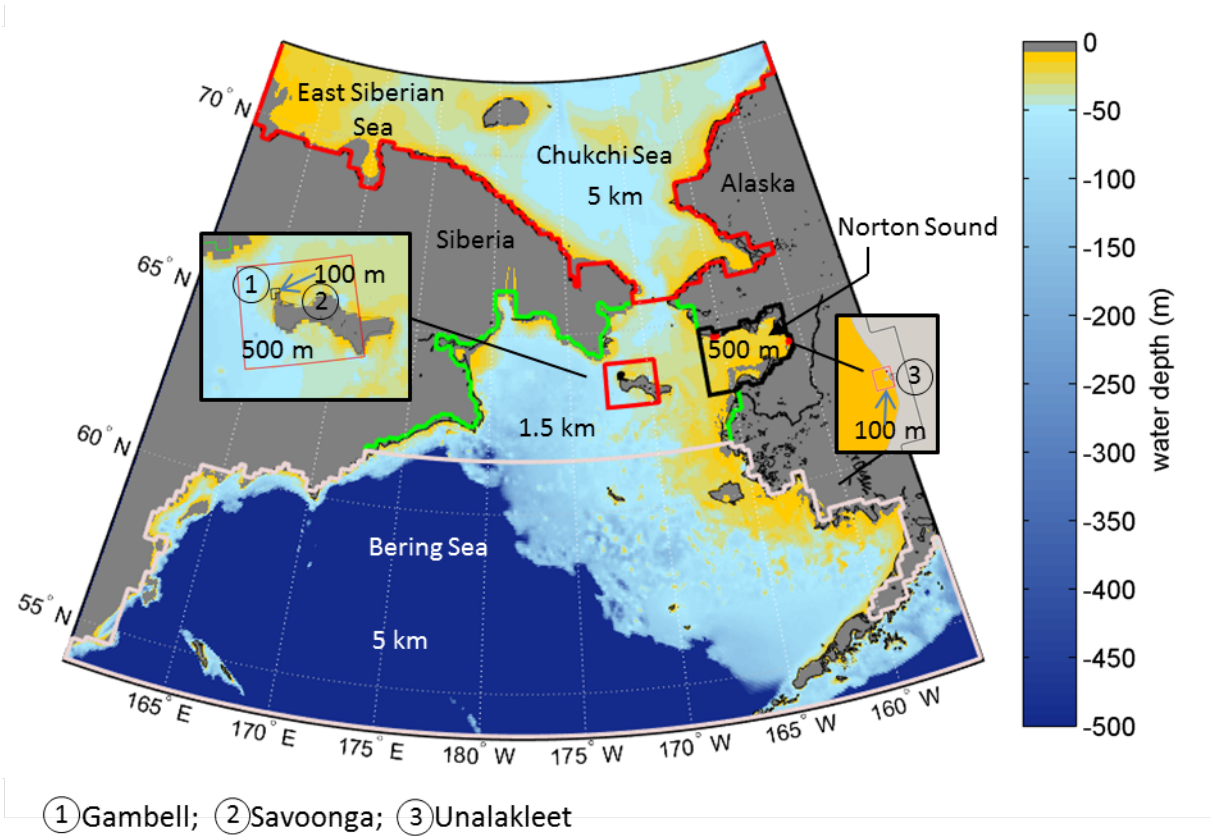


Figure 8. Map showing tide and storm-surge model-grid extent and resolution for the Bering Sea region used in this study. Colored lines delineate grid boundaries. Filled colors represent depths from 1,000 meters (m) (blue) to 0 m (green). km, kilometers.

The bottom friction was set to a constant Chezy value of 65, horizontal eddy viscosity was set at 10 square meters per second ($m^2/s$), and water density was set equal to 1,025 kilograms per cubic meter ($kg/m^3$). For computation of the surface momentum flux, a set of wind stress drag ($C_d$) coefficients related to the windspeed were tested. The magnitude of $C_d$ approximately increases linearly with increasing windspeed and is often approximated with empirically fit data (Garret, 1977 and Charnock, 1955, fig. 9). These linear formulae indicate a maximum $C_d$ of ~$3\times10^{-3}$ for windspeeds less than 30 m/s. Winds blowing over water with sea ice typically exhibit higher $C_d$ (Macklin, 1983; Walter and Overland, 1984), and in the Bering Sea, average conditions of $2.6\times10^{-3}$ to $3.6\times10^{-3}$ have been measured (Macklin, 1983; Walter and Overland, 1984). These higher values are supported by storm-surge modeling studies of the Bering, Chukchi, and Beaufort Seas that have resorted to higher $C_d$ values (Henry and Heaps, 1976; Kowalik, 1984). In the recent work of Chapman and others (2009), $C_d$ was prescribed with the Garratt (1977) formulation but with a spatially varying lower limit set by an empirical equation relating sea-ice concentrations to $C_d$ (Birnbaum and Lupkes, 2002; Garbrecht and others, 2002). In that relation, the effect of sea-ice concentration on $C_d$ is symmetrical such that the maximum $C_d$ ($2.5\times10^{-3}$) occurs with 50 percent ice coverage. Using this approach and assuming a constant 50 percent ice coverage, $C_d$ remains constant at windspeeds as much as of 26 m/s. The Delft3D model employed for this study does not allow for spatially varying $C_d$ fields, and thus a linear relation was employed with a lower limit set at $3.0\times10^{-3}$ and an upper limit defined by the mean of the Charnock (1955) and Garrett (1977) formulations for the 10-m height windspeed ($U_{10}$) of 60 m/s (fig. 9). The

relatively high lower limit was settled on in consideration of drag measurements in the Bering Sea (Macklin, 1983; Walter and Overland, 1984) and iterative comparisons of simulated and measured water levels.

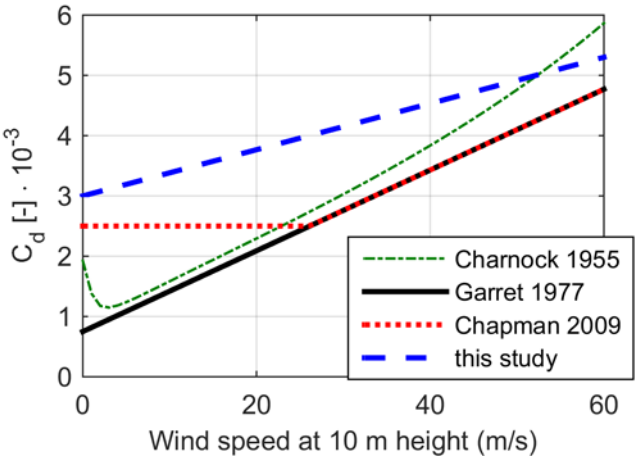


Figure 9. Graph of wind drag coefficient ($C_d$) at 10-meter (m) height as a function of 10-m windspeed ($U_{10}$) according to Charnock (1955; green dash-dot line, using a Charnock constant of 0.025; for example, Vatvani and others, 2013), Garret (1977; black solid), and Chapman (2009) assuming 50 percent sea-ice coverage (red dashed line, and this study (dashed blue).

### Winds and Atmospheric Pressures

In Chapman and others (2009), surface meteorological data, including composite wind, pressure, and ice-concentration fields from Oceanweather (2006), were used to force the storm-surge model. The Oceanweather (2006) dataset was generated by blending point-source meteorological station data into QuicksSCAT satellite data and background wind fields from the National Centers for Environmental Prediction–National Center for Atmospheric Research (NCEP-NCAR). The dataset accounts for orographic steering along coastlines and continuously covers the years 1985 to 2004, with additional time stamps from 1954 to 1984 for selected hindcast storm events.

For this assessment, we used a contrasting meteorological dataset, the North American Regional Reanalysis (NARR) dataset (Earth System Research Laboratory, 2014). The NARR dataset is a high-resolution (0.25° latitude by 0.25° longitude) regional reanalysis of North America that covers the years 1979 to near present (last updated through June 2014 at the time of this report). NARR is a atmosphere and land surface hydrology dataset of the North American region developed from a reanalysis of NCEP/NCAR's global models (Mesinger and others, 2006). The reanalysis is based on addition and assimilation of observational data from monitoring stations, radiosondes, satellites, aircraft reports, and other sources. The surface meteorological data for wind and pressure are available eight times daily over this period. The beginning date also corresponds to the availability of satellite sea-ice measurements that are used to estimate ice concentrations and extent of the seasonal ice pack. A particular benefit of the NARR dataset is that it extends to the near-present, whereas the Oceanweather (2006) dataset was only completed to 2004. This allows for temporal overlap with temporary water-level measurements obtained at Gambell and Unalakleet in 2011 by NOAA and DGGS and storm events that are better documented in the region.

Table 2. Bathymetry data sources used in this study.

| Name/ reference | Description | Dates of collection | Source |
|---|---|---|---|
| Gambell and Unalakleet, Alaska, transects | Cross-shore and alongshore transects extending from the shore to ~10 meters water depth. A total of 16 and 3 transects were available for Gambell and Unalakleet, respectively. Measurements were obtained with a vessel mounted transducer and echo sounder. | July 2013 (Gambell) July 2011 (Unalakleet) | Kinsman (2015). |
| NOAA soundings | Vessel mounted echo sounder. | 1968, 1970 | National Geophysical Data Center (2014). |
| GEBCO08 | A global 1 arc-minute bathymetry dataset generated from quality controlled ship soundings and satellite data. | Most recent data available as of 2008 | General Bathymetric Chart of the Oceans (GEBCO) (2010). |

## Sea-Ice Extents

The presence of sea ice has a measurable effect on the size and onshore arrival time of storm-related surge and wave events (for example, Johnson and Kowalik, 1986). Open-water distance to the ice edge controls wind fetch, which in turn governs wave and surge height. Additionally, the presence of sea ice (partial or full) influences sea-surface roughness and wind drag over water (as discussed in the previous section), which affects wave and storm-surge growth (Birnbaum and Lupkes, 2002; Garbrecht and others, 2002; Andreas and others, 1993). Conversely, the wave field can have a strong influence on the presence and formation of ice, although less is known about this process (Broström and Christensen, 2008).

Weekly mean sea-ice concentrations compiled by NOAA's Earth System Research Laboratory (http://www.esrl.noaa.gov/psd/) were used in this study to define the timing of the open-water season and fetch available for surge and wave growth. The NOAA_OI_SST_V2 dataset includes sea-ice concentrations on a 1.0° global grid starting in October 1981 through November 2014. Only the end of the open-water season is included in the year 1981, and thus for this study, that year was augmented with the first day of open water from 1982 for a complete database spanning years 1981 through 2014. For implementation of the surge and wave models, a time-varying extent of the ice pack was required; this was done by assigning zero windspeed values at grid cells where sea-ice concentrations were greater than 15 percent.

## Wave Model

Propagation of waves to the nearshore was accomplished with the SWAN model. SWAN is a spectral wave model capable of simulating wind-wave growth, propagation, refraction, dissipation, and depth-induced breaking (Booij and others, 1999). Since its initial release in 1998, the model has become a widely used tool for offshore and nearshore wave calculations.

Two sets of grids were generated for the Gambell and Unalakleet regions (fig. 10). Each set consisted of three nested grids ranging in resolution from 500 m in the offshore region to 33 m in the nearshore. In all grids, 10° direction bins and 36 frequencies spaced log-normally from 0.05 to 1.00 hertz (Hz) were used. The bottom friction coefficient was set to 0.067 $m^2/s$ (Bouws and Komen, 1983), white-capping was calculated with the Komen and others (1984) formulation, and depth-induced breaking was calculated with the Battjes and Janssen (1978) formulation. Bathymetry employed in the

wave-model grids were identical to those used in the tide and storm-surge models. All grids were solved in the spherical coordinate system and run in a stationary mode.

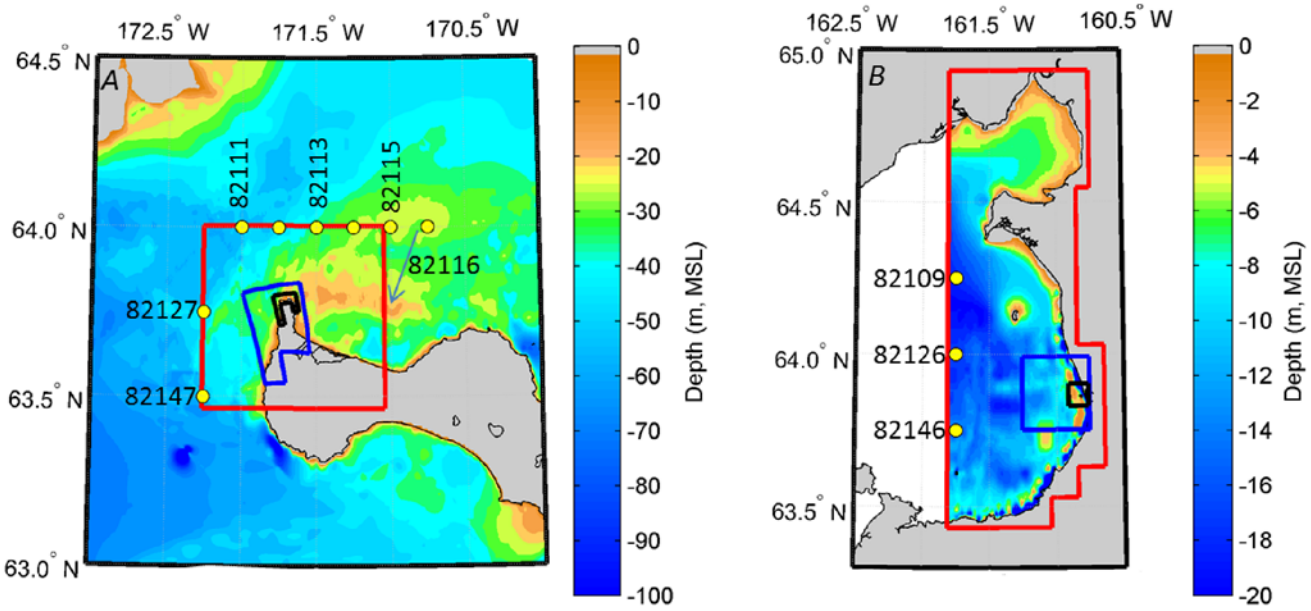


Figure 10. Maps showing wave-model grids used in this study for Bering Sea study sites, Alaska. *A*, Series of nested rectilinear and curvilinear wave grids at Gambell. *B*, Series of nested rectilinear wave grids at Unalakleet. The red, blue, and black outlines define limits of 500-meter (m), 100-m, and 33-m resolution grids, respectively. Yellow circles and station names denote locations of offshore boundary conditions obtained from the U.S. Army Corps of Engineers Wave Information Study (WIS; Jensen and others, 2010). Spatial- and time-varying winds from Earth System Research Laboratory (2014) were also applied to the model domains to simulate local wave growth. MSL, mean sea level.

Wave hindcasts available from the U.S. Army Corps of Engineers Wave Information Study (WIS; Jensen and others, 2010) were used as boundary conditions to the nearshore wave models. The WIS database includes continuous, hourly time-series outputs from 1985 through 2012 for the Chukchi and Bering Seas. Parametric wave descriptors (wave heights, wave directions, and periods) derived from 11 WIS output points were applied along the open boundaries of the Gambell and Unalakleet SWAN grids; these were represented in spectral space with a Joint North Sea Wave Project (JONSWAP, Hasselman and others, 1973) shape and a 3.3 peak enhancement factor. WIS wave hindcasts differ from the wave calculations performed herein in that they were calculated with the WAM Cycle 4.5.1C model (Komen and others, 1994; Gunther and others, 1992) in a nonstationary mode over a 0.25° grid encompassing the area slightly larger than the storm-surge model grid developed for this study. Additionally, the WIS model was forced with Oceanweather wind and pressure fields; the same winds and pressures that were used to simulate storm surges along the west coast of Alaska by Chapman and others (2009).

### Wave-Runup Model

Nearshore hydrodynamics, wave setup, and total runup were simulated with the XBeach-G model (McCall and others, 2014). The model is an extension of the original storm-impact model for sand coasts (Roelvink and others, 2009) and includes a nonhydrostatic solver that resolves both incident and infragravity wave runup. The model was run in a cross-shore transect mode, without morphodynamic updating in a similar manner to that done by McCall and others (2014).

Six cross-shore transects (GC1-GC6) along the west and north shores of Gambell and ranging in elevation from $z$=−15 m to about $z$=+10 m (NAVD88) were defined for Gambell (fig. 3*B*). Profile elevation data were interpolated from a compiled digital elevation model (DEM) generated by DGGS consisting of high-resolution photogrammetric digital elevation data and profile measurements (N. Kinsman, DGGS, written commun., August 2014).

For Unalakleet, four profiles (U7, U13, U15, U16) identified by Kinsman and DeRaps (2012) were used in the simulations (fig. 5*A* and *B*). Subaerial profile measurements in that report were supplemented with bathymetric data obtained by DGGS in 2011 (N. Kinsman, DGGS, written commun., August 2014). Bed-level data of transect U13 were adjusted and projected shore-normal, as is necessary for application of the cross-shore runup model.

Limited data are available for the local grain size and hydraulic conductivity at Unalakleet and Gambell. The median ($D_{50}$) and 90-percent ($D_{90}$) grain sizes were estimated to be 0.0150 and 0.0225 m, respectively, at Gambell (N. Kinsman, DGGS, written commun., May 2014). Based on similarity with the Slapton Sands gravel barrier in the United Kingdom, a hydraulic conductivity of 0.01 m/s was assumed. The bottom of the permeable gravel aquifer was assumed to be at the toe of the gravel barrier, at approximately $z$=−15 m. The groundwater level was initialized at the level of the offshore surge.

At Unalakleet the $D_{50}$ and $D_{90}$ grain sizes were estimated to be 0.0030 and 0.0045 m, respectively (N. Kinsman, DGGS, written commun., May 2014). Based on similarity with the Loe Bar gravel barrier in the United Kingdom, a hydraulic conductivity of 0.005 m/s was assumed. The bed is assumed to be homogenously permeable for the whole model depth. Sensitivity simulations with the bottom of the aquifer at the toe of the gravel barrier ($z$=−1m NAVD88) showed no appreciable difference in runup levels. The groundwater level was initialized at MSL in all simulations. Depending on the cross-shore transect and wave conditions during the storm, the offshore boundaries of the models were placed in shallow water where $kh$<1.5 (where $k$ is the wavenumber and $h$ is the water depth); this resulted in offshore transect boundaries at z=−2 m NAVD88. The shallow offshore endpoints were selected in consideration of the predominantly mild wave conditions (SWH<1.2 m; $T_p$ ~4 s) deduced from simulation of wave propagation and wave growth across Norton Sound. The mild wave conditions are discussed later in the results section of this report.

Thirty storms were simulated on each profile at Gambell and Unalakleet, except for profile GC4 at Gambell, where 60 storms were simulated—30 from the west and 30 from the north. In total, 210 and 120 wave-runup simulations were carried out for Gambell and Unalakleet, respectively. The boundary conditions for the storms consisted of time-varying water levels (storm surge, without tide) and wave conditions (SWHs, $T_p$, and $D_p$, peak direction).

## Evaluation of Model Skill

The ability of the model to reproduce observed water levels were evaluated by computing the root-mean-square-error (*rmse*) and skill scores (*skill*). The *rmse* was calculated with

$$rmse = \frac{1}{N}\sqrt{\sum_{t=1}^{N}(\eta_{\mathrm{mod}} - \eta_{\mathrm{obs}})^2} \quad (1)$$

where $\eta_{\mathrm{mod}}$ and $\eta_{\mathrm{obs}}$ are the modeled and observed water levels, respectively, $N$ is the total number of points or timesteps, and $t$ represents the time-step index. The *rmse* represents the sample standard deviation of the difference between predicted and observed values; smaller *rmse* values illustrate better fits. The second statistic used for model evaluation in this study is the skill score defined as (Willmott, 1981):

$$skill = 1 - \frac{\sum_{i=1}^{N} |\eta_{\mathrm{mod}} - \eta_{\mathrm{obs}}|^2}{\sum_{i=1}^{N} [|\eta_{\mathrm{mod}} - \bar{\eta}_{\mathrm{obs}}| + |\eta_{\mathrm{obs}} - \bar{\eta}_{\mathrm{obs}}|]^2} \quad (2)$$

where over-bars indicate time-averaged values. The skill score ranges from 0 to 1, with a skill score of 1 indicating perfect agreement.

## Tide Model

Three permanent NOAA tide gauges exist within the Bering Sea region of Alaska and are located at Nome, Port Moller, and St. Paul Island (fig. 1). The model was run for the month of December 2013 and compared to published predicted time-series and tidal constituents (table 3 and fig. 11). Constituent amplitudes were calculated from the modeled tide time-series using t-tide (Pawlowicz, 2002). The skill score of time-series data was rather good at greater than 0.94, but *rmse* ranged from 5 cm at Nome (~16 percent of the full tide range, 0.32 m) to nearly 30 cm at Port Moller (~6 percent of the full tide range, 2.25 m). The two largest constituents, $M_2$ (principal lunar semidiurnal) and $K_1$ (lunar diurnal) differ by as little as 2 cm ($M_2$ at Nome) to as much as 13 cm at Port Moller. Although improvements could be made to the tide model (for example, better representation of bed roughness, boundary conditions, and other factors), further efforts were not taken because tide simulations are not the primary focus of this study and the results indicate that the basinwide model response is acceptable.

Table 3. Comparison of tidal-constituent amplitudes modeled (mdl) in this study with published (http://tidesandcurrents.noaa.gov)values (meters) for permanent National Oceanic and Atmospheric Administration (NOAA) tide gauges in the Bering Sea region of Alaska.

[Tidal-constituents: $M_2$, principal lunar semidiurnal; $N_2$, larger lunar elliptic semidiurnal; $K_1$ and $O_1$, lunar diurnal]

| Tide gauge | $M_2$ | | $K_1$ | | $N_2$ | | $O_1$ | |
|---|---|---|---|---|---|---|---|---|
| | NOAA | mdl | NOAA | mdl | NOAA | mdl | NOAA | mdl |
| Nome | 0.12 | 0.10 | 0.09 | 0.06 | 0.04 | 0.03 | 0.07 | 0.04 |
| St. Paul Island | 0.25 | 0.22 | 0.29 | 0.35 | 0.09 | 0.08 | 0.20 | 0.18 |
| Port Moller | 1.03 | 0.89 | 0.65 | 0.83 | 0.32 | 0.28 | 0.40 | 0.37 |

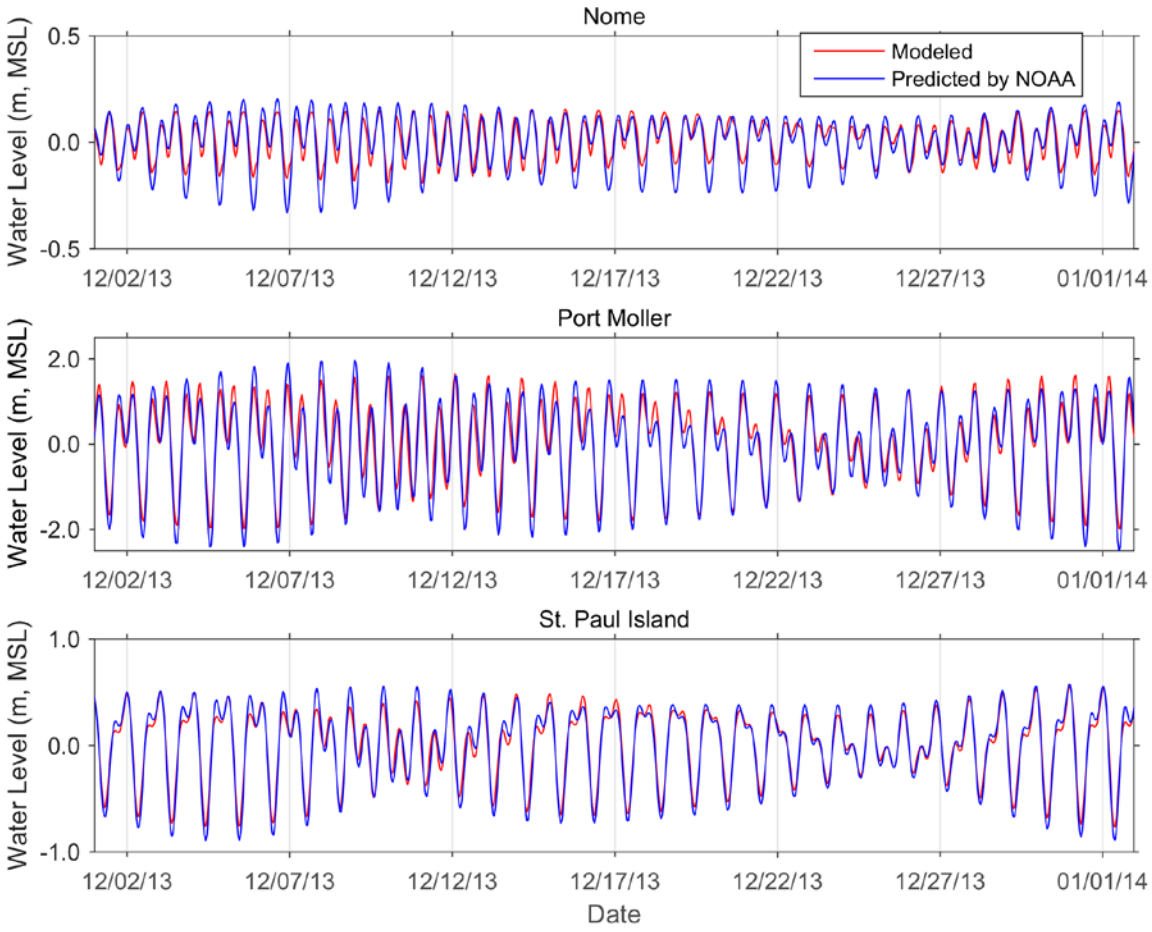


Figure 11. Graphs showing time-series comparison between tides modeled in this study and tides predicted by National Oceanic and Atmospheric Administration (NOAA) at Nome, Port Moller, and St. Paul Island, Alaska. m, MSL, meters relative to mean sea level.

## Storm-Surge Model

Water-level measurements in the vicinity of Gambell, Savoonga, and Unalakleet are available from NOAA for the 2011 open-water season (http://tidesandcurrents.noaa.gov, table 4). The first 2 months of this dataset (June through July 2011) were used to calibrate the storm-surge model; the latter 2 months from August through the first week of October 2011 were used to assess the skill of the model. A low-pass filter was applied to each of the time-series observations to separate the tide signal from other water-level fluctuations (hereafter referred to as nontidal residuals, NTRs). NTRs are water-level fluctuations due to winds (wind setup or set-down), atmospheric pressure gradients, and other larger scale circulation dynamics. NTRs include storm-surge levels during times of high winds and low pressures (that is, during storms). Because residual tide fluctuations remained in the observation data after subtracting harmonically reconstructed tidal time-series, a low-pass filter was instead used to extract the NTRs from the full observation record.

Table 4. National Oceanic and Atmospheric Administration (NOAA) water-level measurement locations and dates at Gambell, Savoonga, and Unalakleet, Alaska (NOAA, 2014).

| Site name | Latitude | Longitude | Observation dates |
|---|---|---|---|
| Gambell/Akeftapak | 63.71833 | -171.64500 | June 13, 2011–Oct. 7, 2011 |
| Savoonga | 63.67833 | -170.53667 | June 23, 2011–Oct. 8, 2011 |
| Unalakleet | 63.87167 | -160.78333 | June 22, 2011–Oct. 11, 2011 |

Inspection of time-series plots that compare modeled and measured NTRs indicate that the patterns of wind setup and setdown (lowering of the water level) are well captured (fig. 12). The model somewhat over and under predicts the setup and setdown events, respectively, but overall shows a reasonable fit. Skill scores are somewhat low for Gambell/Akeftapak and Savoonga (0.63 and 0.69, respectively; table 5). However, NTR fluctuations were small (±~0.30 m), thus limiting the validity of using this time-period for assessment of the models ability of capturing extreme events near St. Lawrence Island. The skill score is substantially better at Unalakleet (0.85), where a maximum NTR water level of 0.89 m was measured. The model over predicted this event by 0.27 m.

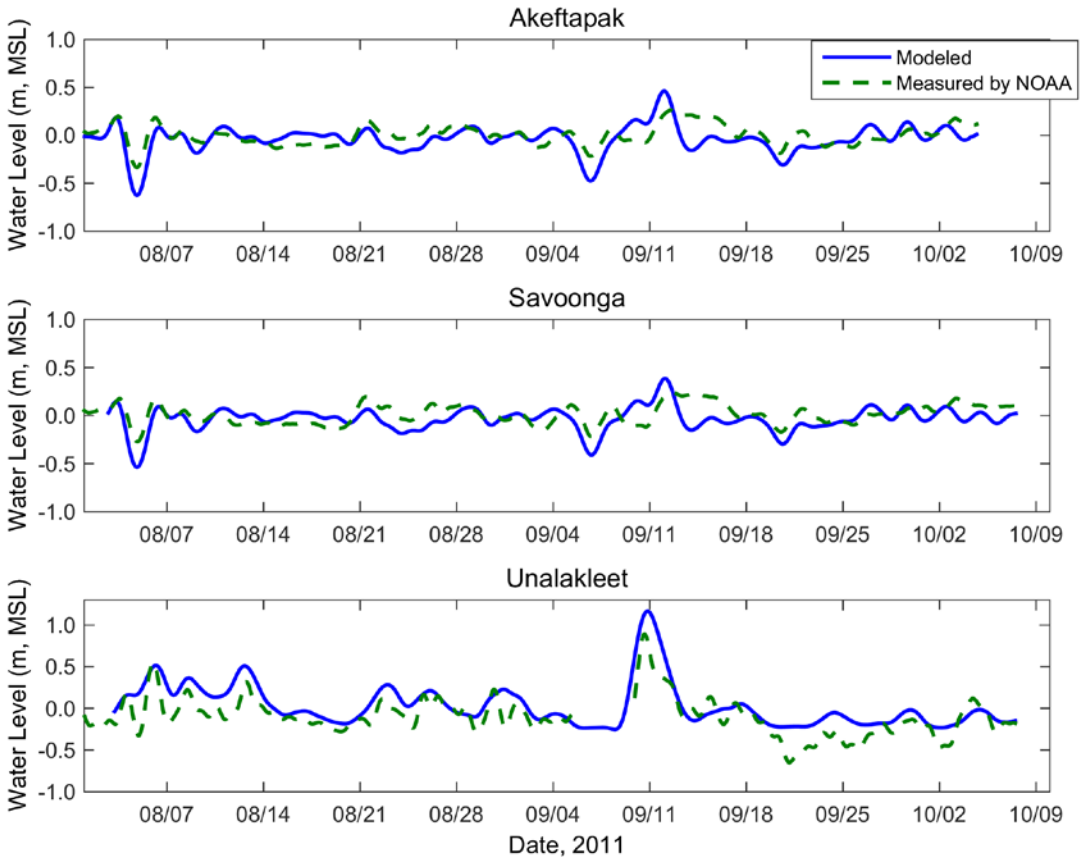


Figure 12. Graphs comparing nontidal residuals modeled in this study with of nontidal residuals measured by the National Oceanic and Atmospheric Administration (NOAA, http://tidesandcurrents.noaa.gov) at Akeftapak (east side of Gambell), Savoonga, and Unalakleet, Alaska, from August through the first week of October 2011. m, MSL, meters relative to mean sea level.

Table 5. Summary of model skill estimates for this study at Akeftapak (east side of Gambell), Savoonga, and Unalakleet, Alaska.
[*rmse*, root-mean-square-error; *skill*, skill score; *N*, total number of points or timesteps]

| Site name | *skill* | *rmse* | *N* |
|---|---|---|---|
| Gambell/Akeftapak | 0.69 | 0.13 | 1,553 |
| Savoonga | 0.63 | 0.13 | 1,580 |
| Unalakleet | 0.85 | 0.20 | 1,459 |

Although the 0.89 m water level measured at Unalakleet is of some significance, it does not represent a significant storm surge, and hence it is prudent to check the model against extreme events captured at Nome where there has been a permanent tide gauge since 1992. Modeled and measured water levels are plotted for the November 2011 storm in figure 13*A*. This storm affected most of Norton Sound including Unalakleet (Kinsman and DeRaps, 2012). The overall shape is well captured but the peak is underestimated. The maximum storm surge was 2.75 m above MSL, whereas the modeled storm surge was 2.11 m. Two other storms of note (as listed in Chapman and others, 2009) since 1992, for which observations exist at Nome, were better represented with differences of 0.28 m and 0.06 m for the October 1992 and 2004 storms, respectively (observed minus modeled, fig. 13*B*).

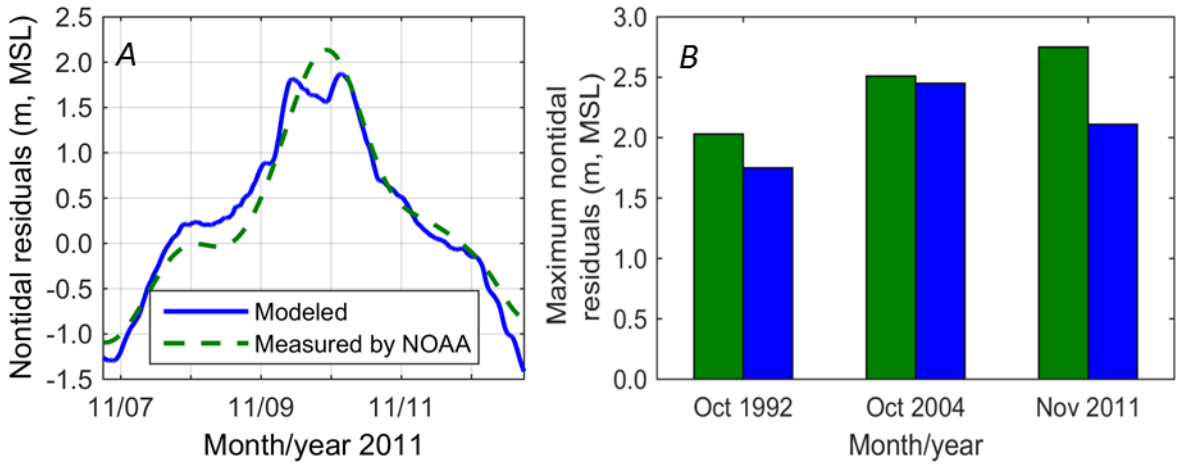


Figure 13. Graphs showing storm-surge levels modeled in this study and measured (http://tidesandcurrents.noaa.gov) at Nome, Alaska. *A*, Time-series comparison of the November 2011 Bering Sea storm (tide removed from measurement data). *B*, Bar graph showing maximum measured (blue) and modeled (green) storm-surge levels for three Bering Sea storms (including the 2011 storm) for which observational data exists and overlaps with the modeled time-period. m, MSL, meters relative to mean sea level.

Although no water-level gauge recorded the November 2011 storm at Unalakleet, Kinsman and DeRaps (2012) surveyed the area immediately following that storm and inferred a set of maximum water levels from driftwood, ice, and visible water lines against hard structures. Immediately landward of the Unalakleet River inlet, a peak storm-tide flood level of 2.66±0.04 m MSL was measured by visual identification of the water line on physical infrastructure (table 2 in Kinsman and DeRaps, 2012, point MP14). Model results obtained as part of this study compare well with their observations. The modeled

hindcast November 2011 storm reached a maximum surge level of 2.54 m MSL and 2.58 m MSL with and without astronomic tides, respectively (fig. 14*A*). Astronomic tide levels were hindcast to have been just a few centimeters high when the peak of the surge arrived at Unalakleet.

The Unalakleet community was fortunate in that the November 2011 storm occurred during near zero neap-tide conditions. The maximum tide elevation on November 9, 2011 was ~0.56 m and occurred 6 hours after the peak of the storm surge. Had the storm passed through the area somewhat later (or earlier), the water elevation because of the surge and tides could have been half a meter higher. In contrast, had the storm arrived at the same time but in the year 2014, the storm tide would have been slightly lower as the tides vary from year to year (fig. 14*B*). Had the storm occurred later in the fall or early winter and had the pack ice been away from the coast, the storm tide could have been nearly 1 m higher (fig. 14*C*). Because there are several prominent cycles in the tide signal—for example, the 18.6 year lunar node, and 4-year, annual, monthly, and daily tides—the storm-tide level is intricately dependent on the timing of storm-surge events with respect to tides. It is because of this that storm-surge simulations and return-value statistics are calculated independent of tide levels.

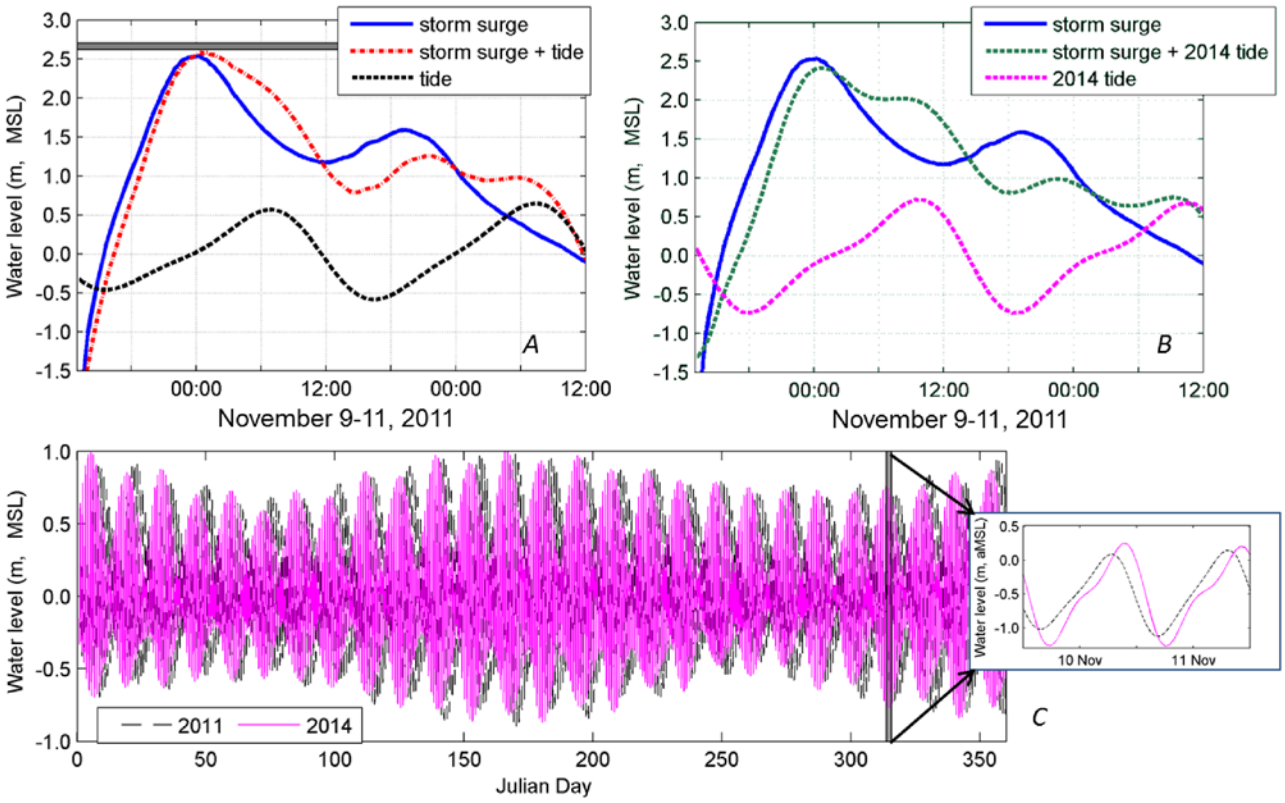


Figure 14. Graphs showing simulated November 9–11, 2011, Bearing Sea storm surge at Unalakleet, Alaska. *A*, Time-series of individual contributions from storm surge (solid blue line), tide (dashed black line), and the combination of storm and tide (dash dot red line, assuming linear superposition of storm surge and astronomic tide). Shaded horizontal bar indicates measured peak storm-tide level (Kinsman and DeRaps, 2012). *B*, The same as in *A* but with tide stage as it occurred in November 2014, shifted by 72 hrs. *C*, Time-series comparison of year-long tide elevations at Unalakleet for 2011 and 2014. Note the larger tidal range and higher maximum tide elevations at the middle and beginning and end of calendar years. Inset shows the 2011 and 2014 tide levels plotted in *A* and *B* but on the same axis. m, MSL, meters relative to mean sea level.

## Wave-Runup Model

As there are no instrumented wave or runup observations available at Gambell and Unalakleet, evaluation of wave conditions and wave runup is done herein by comparing model results with reported visual estimates and elevation measurements of wrack lines. Wave and runup simulations encompass the years 1985 through 2012; the highest SWHs during this time period were estimated to be ~6.5 m (October 1996) at 15-m water depth offshore of Gambell. This is reasonable in consideration of community reports that indicate maximum SWHs of ~8 m that may have occurred in the 1970s (Floodplain Manager, Gambell City Office, written commun., 2011). Model results indicate that all extreme events that impacted the coast approached from the west, consistent with observations reported by long-term local residents (Floodplain Manager, Gambell City Office, written commun., 2011). The November 2011 storm was reported to have caused minor flooding. Model simulations ranked the 2011 storm as the second highest (between 1985 and 2012) with overtopping at three of the six cross-shore profiles simulated (GC2, GC5, and GC6). Model results suggest that overtopping and flooding occurred during a couple additional events in 1996 and 2004 at transects GC1 and GC2. At this time it is uncertain if observational evidence exists for this.

Kinsman and DeRaps (2012) measured total runup heights (runup+surge+tide) in Unalakleet following the November 2011 storm. Near the south end of town, maximum runup heights of 4.82 m to 5.08±0.05 m MSL were derived from landward locations of slush lines and driftwood (Kinsman and DeRaps, 2012; sites MP06 and MP07, table 2). These levels are more than twice as high as those estimated with the model in this study for which a maximum surge+runup for the November 2011 event only reached 2.2 m MSL at transect U16 near the south end of town. The discrepancy is partly due to the fact that storm-surge variations fed to the XBEACH model were taken from the 8-m depth contour, whereas the offshore endpoint of the XBEACH transects were moved to much shallower depths following realization of the very low incident wave conditions. However, the main contributing factor to the underestimate of surge+runup are the low wave heights and consequent runup. The maximum calculated runup was estimated to be 0.7 m above the still-water line for the November 2011 event. The runup estimate was calculated with waves propagated across Norton Sound (). The maximum SWH at the offshore boundary WIS station 82126 (see fig. 10*B* for location) was 2.24 m with a $T_p$ of 7.6 s during the 2011 storm. Using this greater offshore wave condition to force the XBEACH wave model, rather than the smaller nearshore SWHs (less than 1 m) following propagation across Norton Sound, increases wave runup to ~0.88 m above the still-water level. This raises the combined storm surge+runup height to 0.88 m+2.56 m=3.44 m, but this is still more than 1 meter below field observations. The entire time-series of the offshore WIS hindcast time-series from 1985 through 2012 was inspected and found not to exceed 2.7 m at stations 82146 and 82126. As these values seem low, SWHs were compared to ERA Interim (ERA-I), the latest global atmospheric reanalysis produced by the European Centre for Medium Range Weather Forecasts (Dee and others, 2011). ERA-I wave parameters were generated from a fully coupled $0.75^{o}$-resolution atmosphere-ocean wave model and high-resolution reanalysis winds. Post 1990 data include adjustments derived from satellite radar-altimeter wave-height data.

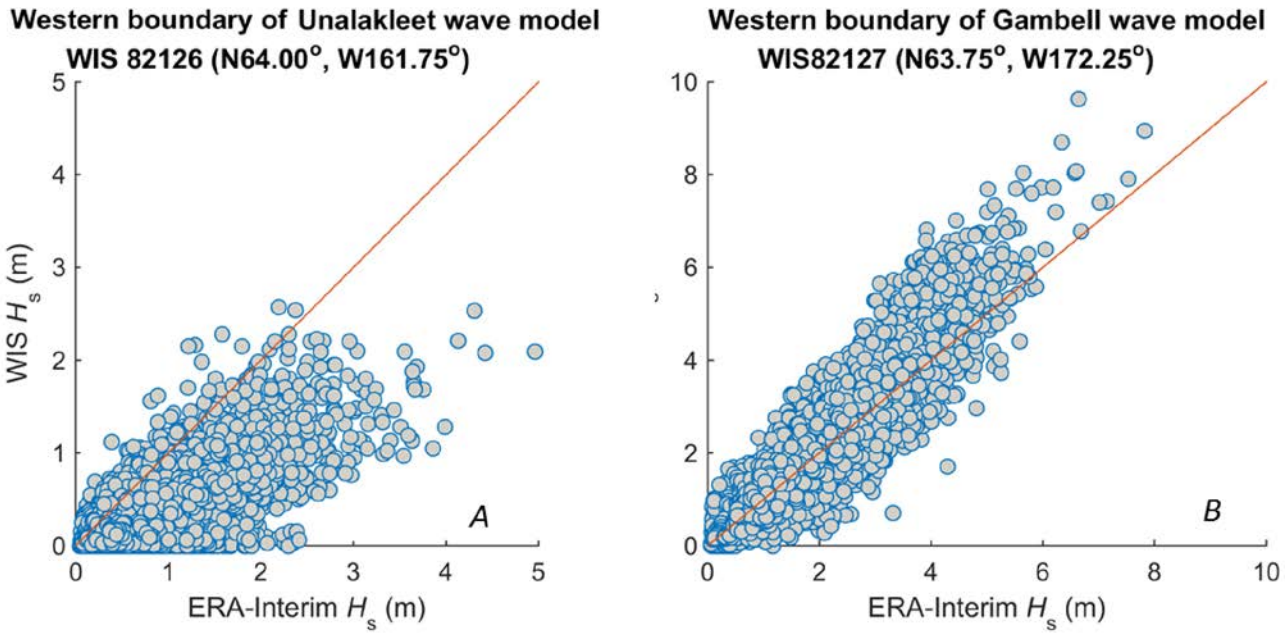


Figure 15. Graphs comparing significant wave heights ($H_S$) hindcast with the Wave Information Study (WIS; Jensen and others, 2010) and ERA-Interim (Dee and others, 2011) models. Two locations from which WIS data were used to drive the wave models are shown—*A*, western boundary of Unalakleet, Alaska, wave model, and *B*, western boundary of the Gambell, Alaska, wave model. Solid lines indicate a perfect (1:1) fit. m, meters.

Compared to ERA-I, the WIS-derived SWHs in combination with the presence of the alongshore bar suggest that the calculated SWHs used at the open boundary of the Unalakleet wave model are radically undervalued, by as much 2.5 m (fig. 15*A*). Conversely, WIS-derived SWHs used at the open boundary of the Gambell wave model are slightly higher than ERA-I (fig. 15*B*) and are likely more representative of true conditions, as ERA-I has been shown to underestimate SWHs compared to buoy observations (for example, Stopa and Cheung, 2014). Thus, the low wave runup heights simulated at Unalakleet for this study are representative of the boundary conditions used but are too low because of undervalued forcing at the open boundary of the wave model. Simulated runup heights at Gambell do not appear to be affected by underestimated boundary conditions.

## Identified Storm Events at St. Lawrence Island and Unalakleet, 1981–2012

### Storm Surges

The storm-surge model was run for 32 years of the open-water season from 1981 through 2012. The open-water season was identified as the time when the mean weekly sea-ice concentration was less than15 percent in the vicinity of St. Lawrence Island and Norton Sound. The end of the open-water season increased by 0.5 days/year over the entire study time (statistically significant at $p<0.05$; fig. 16*A*). Maximum storm-surge elevations (excluding tides) were 2.02 m MSL at the western and northern exposed coasts of Gambell and Savoonga (November 2006) and 3.10 m at Unalakleet (October 2004) (figs. 16*B, C* and tables 6 through 7). Of the sites studied, Unalakleet has the highest storm-surge levels followed by Gambell and Savoonga. Savoonga exhibited just slightly lower surge levels compared to Gambell. Simulation results did not show any appreciable difference between storm-surge elevations on the west and north sides of Gambell. The 90th percentile storm-surge elevations were ~0.45 m at Gambell and Savoonga; the 90th percentile elevation at Unalakleet was nearly twice as high at 1.03 m. The number of annual extreme storm-surge events, counted as those that exceeded the 90th percentile of the 1981–2012 time period, was at most seven but often occurred five or six times during any given year (figs. 16*B, C*). There is no apparent trend of increasing storm-surge height or frequency with respect to time.

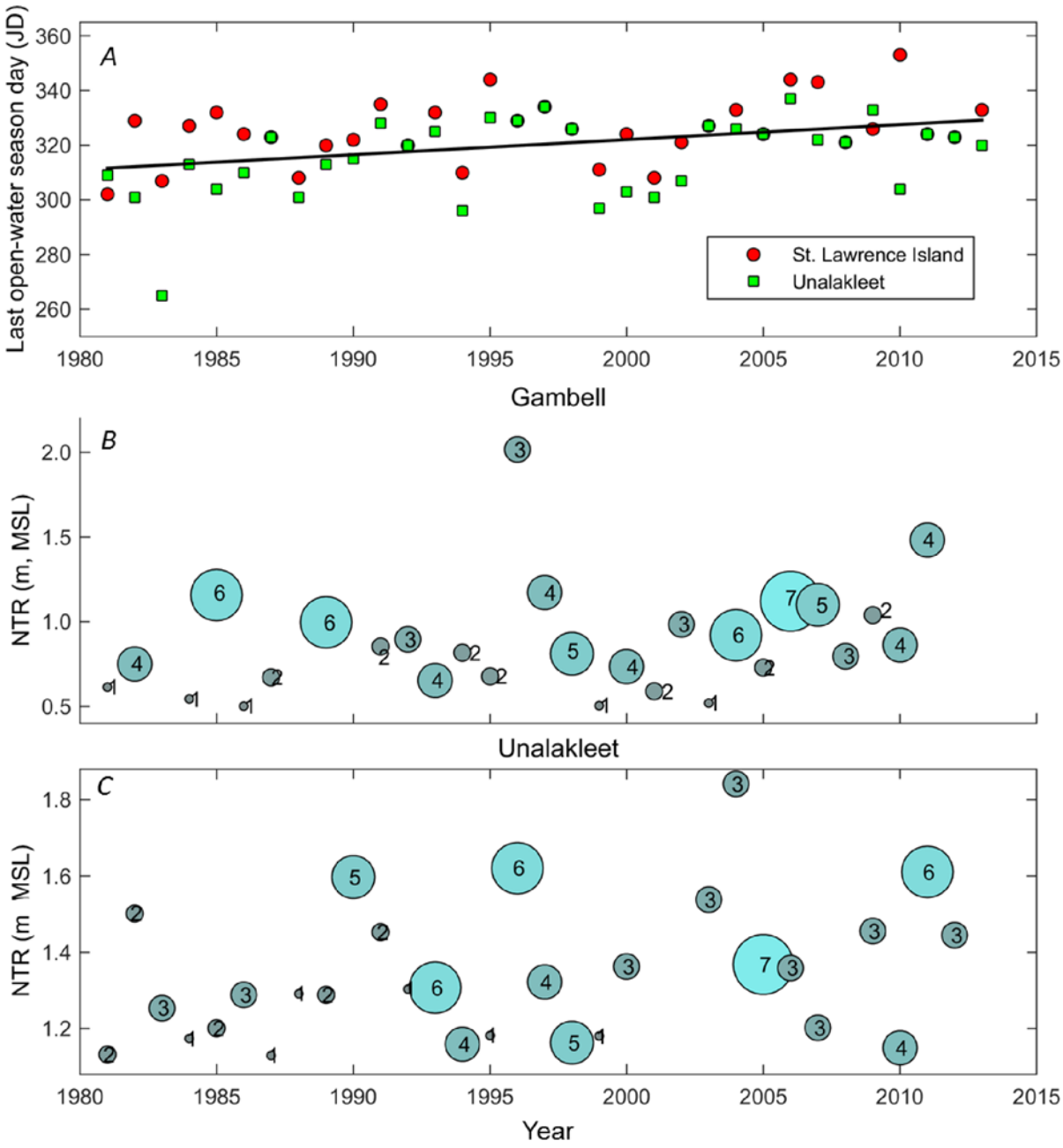


Figure 16. Plots showing change in last day of the open-water season over the past three decades and maximum simulated annual nontidal residual (NTRs) for years 1981 through 2012 for St. Lawrence Island (Gambell and Savoonga) and Unalakleet, Alaska. *A*, Change in last day of open-water season. Black trend line shows linear fit through the last Julian Day (JD) of the open-water season with respect to time. Linear trend line indicates an increase of 0.5 days per year (statistically signficant at the $p<0.05$ level). *B* (Gambell) and *C* (Unalakleet), Circles indicate the maximum annual nontidal residual or surge level simulated during the open water season. Circle size, color hue, and numbers indicate the number of events that exceeded the 90th percentile NTR for the 32-year time period (90th percentiles are 0.45 meters (m), 0.45 m, and 1.03 m for Gambell, Savoonga, and Unalakleet, respectively). Savoonga data are nearly identical to Gambell and so are not explicitly shown here. m, MSL, meters relative to mean sea level.

Storm surges were greatest in response to winds from the northwest quadrant at Gambell and Savoonga (tables 6 through 9). Winds from the southwest and southeast quadrants produced the greatest storm surges at Unalakleet (table 9). Windspeeds and directions listed in tables 6 through 9 were obtained by selecting the highest windspeeds and associated directions from the NARR database for the time of the storm and 1 day preceding the simulated maximum surge level. Although the wind magnitudes and directions are general indications of storm strength and incident direction, the values can be misleading as the surge levels are responses to winds blowing over long durations and large open-water areas as opposed to local short-term conditions. This is particularly noticeable with the wind directions obtained for Unalakleet, which in some instances indicate winds from the east-southeast (ESE) direction overland (note that the incident wind directions are generally consistent with findings in Chapman and others, 2009). In these cases, the local wind direction likely differs somewhat from the wind patterns that caused the storm surge.

Table 6. Data for the 30 largest storm-surge events at the west coast of Gambell, Alaska, between 1981 and 2012.

[m, meters; m/s, meters per second; kPa, kilopascal; N, north; S, south; W, west]

| Rank | Date | Max water level (m) | Minimum sea level pressure (kPa) | Maximum wind | |
|---|---|---|---|---|---|
| | | | | Speed (m/s) | Blowing from |
| 1 | Nov. 15, 1996 | 2.02 | 98.679 | 18.4 | WNW |
| 2 | Nov. 9, 2011 | 1.49 | 95.992 | 19.4 | WSW |
| 3 | Nov. 18, 2011 | 1.17 | 100.181 | 17.5 | WSW |
| 4 | Nov. 14, 1997 | 1.17 | 99.730 | 15.2 | WNW |
| 5 | Nov. 9, 1985 | 1.16 | 102.097 | 12.8 | WSW |
| 6 | Dec. 3, 2006 | 1.12 | 100.605 | 13.5 | WNW |
| 7 | Nov. 30, 2007 | 1.10 | 99.547 | 18.0 | WNW |
| 8 | Jul. 3, 2009 | 1.04 | 100.810 | 14.5 | W |
| 9 | Nov. 26, 2006 | 1.02 | 97.232 | 21.6 | W |
| 10 | Nov. 15, 1989 | 1.00 | 100.000 | 19.4 | WNW |
| 11 | Sep. 11, 2007 | 0.99 | 99.611 | 14.9 | W |
| 12 | Oct. 10, 2002 | 0.98 | 99.179 | 16.5 | WSW |
| 13 | Nov. 22, 2004 | 0.92 | 97.711 | 19.2 | WSW |
| 14 | Nov. 22, 1985 | 0.92 | 101.263 | 11.1 | WNW |
| 15 | Oct. 5, 1992 | 0.89 | 98.410 | 17.3 | NW |
| 16 | May 19, 1997 | 0.87 | 100.075 | 11.4 | WSW |
| 17 | Oct 27, 2010 | 0.86 | 99.420 | 16.0 | WNW |
| 18 | Nov. 12, 1992 | 0.86 | 101.023 | 11.4 | W |
| 19 | Oct. 16, 1991 | 0.86 | 97.776 | 13.1 | SW |
| 20 | Nov. 5, 1994 | 0.82 | 97.809 | 11.0 | WNW |
| 21 | May 17, 1998 | 0.81 | 99.287 | 13.8 | SW |
| 22 | Oct. 28, 2008 | 0.80 | 98.869 | 14.1 | WNW |
| 23 | Nov. 1, 1997 | 0.79 | 99.324 | 16.5 | NNW |
| 24 | Oct 28, 1996 | 0.77 | 98.868 | 18.0 | N |
| 25 | Nov. 8, 1998 | 0.75 | 100.535 | 12.8 | W |
| 26 | Nov. 18, 1982 | 0.75 | 99.712 | 11.6 | WNW |
| 27 | Nov. 4, 1985 | 0.75 | 99.784 | 11.7 | WSW |
| 28 | Oct. 10, 1989 | 0.74 | 98.784 | 15.4 | W |
| 29 | Apr. 13, 1989 | 0.74 | 98.550 | 9.1 | WNW |
| 30 | Nov. 4, 2000 | 0.74 | 100.365 | 18.5 | SW |

Table 7. Data for the 30 largest storm-surge events at the north coast of Gambell, Alaska, between 1981 and 2012.

[m, meters; m/s, meters per second; kPa, kilopascal; N, north; S, south; W, west]

| Rank | Date | Max water level (m) | Minimum sea level pressure (kPa) | Maximum wind | |
|---|---|---|---|---|---|
| | | | | Speed (m/s) | Blowing from |
| 1 | Nov. 15, 1996 | 2.02 | 98.679 | 18.4 | WNW |
| 2 | Nov. 9, 2011 | 1.39 | 95.992 | 19.4 | WSW |
| 3 | Nov. 14, 1997 | 1.17 | 100.181 | 15.2 | WNW |
| 4 | Nov. 9, 1985 | 1.16 | 99.730 | 12.8 | WSW |
| 5 | Nov. 18, 2011 | 1.11 | 102.097 | 17.5 | WSW |
| 6 | Dec. 3, 2006 | 1.10 | 100.605 | 13.5 | WNW |
| 7 | Nov. 30, 2007 | 1.06 | 99.547 | 18.0 | WNW |
| 8 | Jul. 3, 2009 | 1.00 | 100.810 | 14.5 | W |
| 9 | Nov. 15, 1989 | 1.00 | 97.232 | 19.4 | WNW |
| 10 | Oct. 10, 2002 | 0.98 | 100.000 | 16.5 | WSW |
| 11 | Sep. 11, 2007 | 0.96 | 99.611 | 14.9 | W |
| 12 | Nov. 26, 2006 | 0.96 | 99.179 | 21.6 | W |
| 13 | Nov. 22, 2004 | 0.92 | 97.711 | 19.2 | WSW |
| 14 | Nov. 22, 1985 | 0.92 | 101.263 | 11.1 | WNW |
| 15 | Oct. 5, 1992 | 0.89 | 98.410 | 17.3 | NW |
| 16 | May. 19, 1997 | 0.87 | 100.075 | 11.4 | WSW |
| 17 | Nov. 12, 1992 | 0.86 | 99.420 | 11.4 | W |
| 18 | Oct. 16, 1991 | 0.86 | 101.023 | 13.1 | SW |
| 19 | Oct. 27, 2010 | 0.82 | 97.776 | 16.0 | WNW |
| 20 | Nov. 5, 1994 | 0.82 | 97.809 | 11.0 | WNW |
| 21 | May. 17, 1998 | 0.81 | 99.287 | 13.8 | SW |
| 22 | Nov. 1, 1997 | 0.79 | 98.869 | 16.5 | NNW |
| 23 | Oct. 28, 2008 | 0.78 | 99.324 | 14.1 | WNW |
| 24 | Oct. 28, 1996 | 0.77 | 98.868 | 18.0 | N |
| 25 | Nov. 8, 1998 | 0.75 | 100.535 | 12.8 | W |
| 26 | Nov. 18, 1982 | 0.75 | 99.712 | 11.6 | WNW |
| 27 | Nov. 4, 1985 | 0.75 | 99.784 | 11.7 | WSW |
| 28 | Oct. 10, 1989 | 0.74 | 98.784 | 15.4 | W |
| 29 | Apr. 13, 1989 | 0.74 | 98.550 | 9.1 | WNW |
| 30 | Nov. 4, 2000 | 0.74 | 100.365 | 18.5 | SW |

Table 8. Data for the 30 largest storm-surge events at Savoonga, Alaska, between 1981 and 2012.
[m, meters; m/s, meters per second; kPa, kilopascal; N, north; S, south; W, west]

| Rank | Date | Max water level (m) | Minimum sea level pressure (kPa) | Maximum wind | |
|---|---|---|---|---|---|
| | | | | Speed (m/s) | Blowing from |
| 1 | Nov. 15, 1996 | 2.02 | 99.004 | 16.5 | WNW |
| 2 | Nov. 9, 2011 | 1.41 | 96.227 | 19.2 | WSW |
| 3 | Nov. 14, 1997 | 1.17 | 100.364 | 15.0 | WNW |
| 4 | Nov. 9, 1985 | 1.16 | 99.853 | 14.4 | W |
| 5 | Nov. 18, 2011 | 1.12 | 100.685 | 12.8 | WNW |
| 6 | Dec. 3, 2006 | 1.11 | 102.212 | 17.2 | WSW |
| 7 | Nov. 30, 2007 | 1.02 | 99.720 | 18.1 | WNW |
| 8 | Jul. 3, 2009 | 1.01 | 100.950 | 14.2 | WNW |
| 9 | Nov. 15, 1989 | 1.00 | 97.527 | 19.5 | WNW |
| 10 | Oct. 10, 2002 | 0.98 | 100.020 | 15.0 | W |
| 11 | Sep. 11, 2007 | 0.98 | 99.708 | 14.8 | WNW |
| 12 | Nov. 26, 2006 | 0.93 | 99.448 | 20.8 | W |
| 13 | Nov. 22, 2004 | 0.92 | 97.746 | 18.7 | W |
| 14 | Nov. 22, 1985 | 0.92 | 101.378 | 12.1 | WNW |
| 15 | Oct. 5, 1992 | 0.89 | 98.771 | 18.9 | NNW |
| 16 | May. 19, 1997 | 0.87 | 100.175 | 11.5 | W |
| 17 | Nov. 12, 1992 | 0.86 | 99.654 | 12.3 | WNW |
| 18 | Oct. 16, 1991 | 0.86 | 100.939 | 12.1 | SW |
| 19 | Oct. 27, 2010 | 0.84 | 98.053 | 15.7 | NW |
| 20 | Nov. 5, 1994 | 0.82 | 98.065 | 12.6 | WNW |
| 21 | May. 17, 1998 | 0.81 | 99.265 | 12.4 | WSW |
| 22 | Nov. 1, 1997 | 0.80 | 99.467 | 14.7 | WNW |
| 23 | Oct. 28, 2008 | 0.79 | 99.116 | 15.6 | NW |
| 24 | Oct. 28, 1996 | 0.77 | 99.226 | 17.7 | N |
| 25 | Nov. 8, 1998 | 0.75 | 100.628 | 11.2 | W |
| 26 | Nov. 18, 1982 | 0.75 | 99.942 | 12.6 | NW |
| 27 | Nov. 4, 1985 | 0.75 | 99.725 | 11.1 | WSW |
| 28 | Oct. 10, 1989 | 0.74 | 98.850 | 14.9 | W |
| 29 | Apr. 13, 1989 | 0.74 | 98.785 | 10.2 | NW |
| 30 | Nov. 4, 2000 | 0.74 | 100.328 | 15.6 | SW |

Table 9. Data for the 30 largest storm-surge events at Unalakleet, Alaska, between 1981 and 2012.
[m, meters; m/s, meters per second; kPa, kilopascal; N, north; S, south; W, west]

| Rank | Date | Max water level (m) | Minimum sea level pressure (kPa) | Maximum wind | |
|---|---|---|---|---|---|
| | | | | Speed (m/s) | Blowing from |
| 1 | Oct. 19, 2004 | 3.10 | 98.408 | 14.3 | ESE |
| 2 | Oct. 28, 1996 | 2.55 | 101.237 | 8.6 | SSE |
| 3 | Nov. 10, 2011 | 2.53 | 98.742 | 14.8 | E |
| 4 | Sep. 6, 1990 | 2.49 | 99.313 | 14.3 | SW |
| 5 | Nov. 9, 2003 | 2.34 | 98.501 | 14.3 | SW |
| 6 | Oct. 19, 1982 | 2.25 | 101.149 | 10.2 | S |
| 7 | Aug. 27, 1990 | 2.24 | 99.663 | 12.1 | SW |
| 8 | Nov. 12, 2009 | 2.14 | 96.895 | 14.0 | WSW |
| 9 | Oct. 22, 1991 | 2.13 | 101.474 | 10.3 | SSW |
| 10 | Aug. 25, 2012 | 2.11 | 99.792 | 9.4 | WSW |
| 11 | Nov. 22, 2003 | 1.96 | 99.514 | 9.8 | SE |
| 12 | Sep. 23, 2005 | 1.92 | 98.521 | 13.8 | S |
| 13 | Sep. 2, 2000 | 1.91 | 100.788 | 11.5 | SW |
| 14 | Oct. 28, 2006 | 1.90 | 101.463 | 9.3 | S |
| 15 | Nov. 15, 1996 | 1.86 | 101.176 | 10.3 | ESE |
| 16 | Oct. 4, 1997 | 1.80 | 99.413 | 10.7 | SW |
| 17 | Oct. 2, 1993 | 1.77 | 98.383 | 15.1 | SSW |
| 18 | Oct. 6, 1992 | 1.76 | 98.825 | 11.8 | SSE |
| 19 | Sep. 1, 2009 | 1.73 | 100.128 | 9.9 | SSW |
| 20 | Aug. 15, 1988 | 1.73 | 100.574 | 10.8 | SSW |
| 21 | Oct. 19, 1989 | 1.72 | 98.654 | 11.3 | SSE |
| 22 | Jul. 20, 1986 | 1.72 | 102.153 | 9.2 | SW |
| 23 | Aug. 4, 1997 | 1.67 | 100.697 | 9.1 | SSE |
| 24 | Oct. 5, 1983 | 1.63 | 101.074 | 8.5 | SW |
| 25 | Dec. 2, 2006 | 1.58 | 101.252 | 9.2 | SW |
| 26 | Aug. 2, 1996 | 1.51 | 99.863 | 9.9 | SW |
| 27 | Oct. 9, 2007 | 1.51 | 100.678 | 8.5 | SSW |
| 28 | Nov. 10, 1985 | 1.50 | 100.171 | 9.5 | SE |
| 29 | Nov. 17, 1990 | 1.47 | 99.911 | 6.0 | ESE |
| 30 | Oct. 1, 1983 | 1.46 | 97.660 | 10.5 | SE |

## Storm Surge Plus Wave Runup

The 30 highest water levels ($z_{max}$) estimated to have been reached due to the dynamic combination of storm surge and wave runup (no tides) are listed in tables 10 and 11 for one transect each on the west and north facing coasts of Gambell and one transect each north of Unalakleet and at the south end of the community. Results for all six transects at Gambell and four transects at Unalakleet are summarized in figures 17 and 18. The events are limited to the time period between 1985 and 2012; the beginning date represents the year in which time-series offshore wave data were available. In all cases of the same storm event, $z_{max}$ is greater on the western exposed coast of Gambell compared to the north coast, in some cases more than twice as high. For a given storm, SWHs at the 15-m isobaths are slightly higher on the north side compared to the west side; however, due to the incidence angles and more shallow nearshore bathymetry (fig. 17, compare for example profile GC2 with GC6), the waves on the north coast dissipate more energy as they refract and break further from the coast, resulting in lower runup heights. Peak wave periods are all more than 9 seconds, indicating that the highest energy is contained in swell waves generated from distant storms.

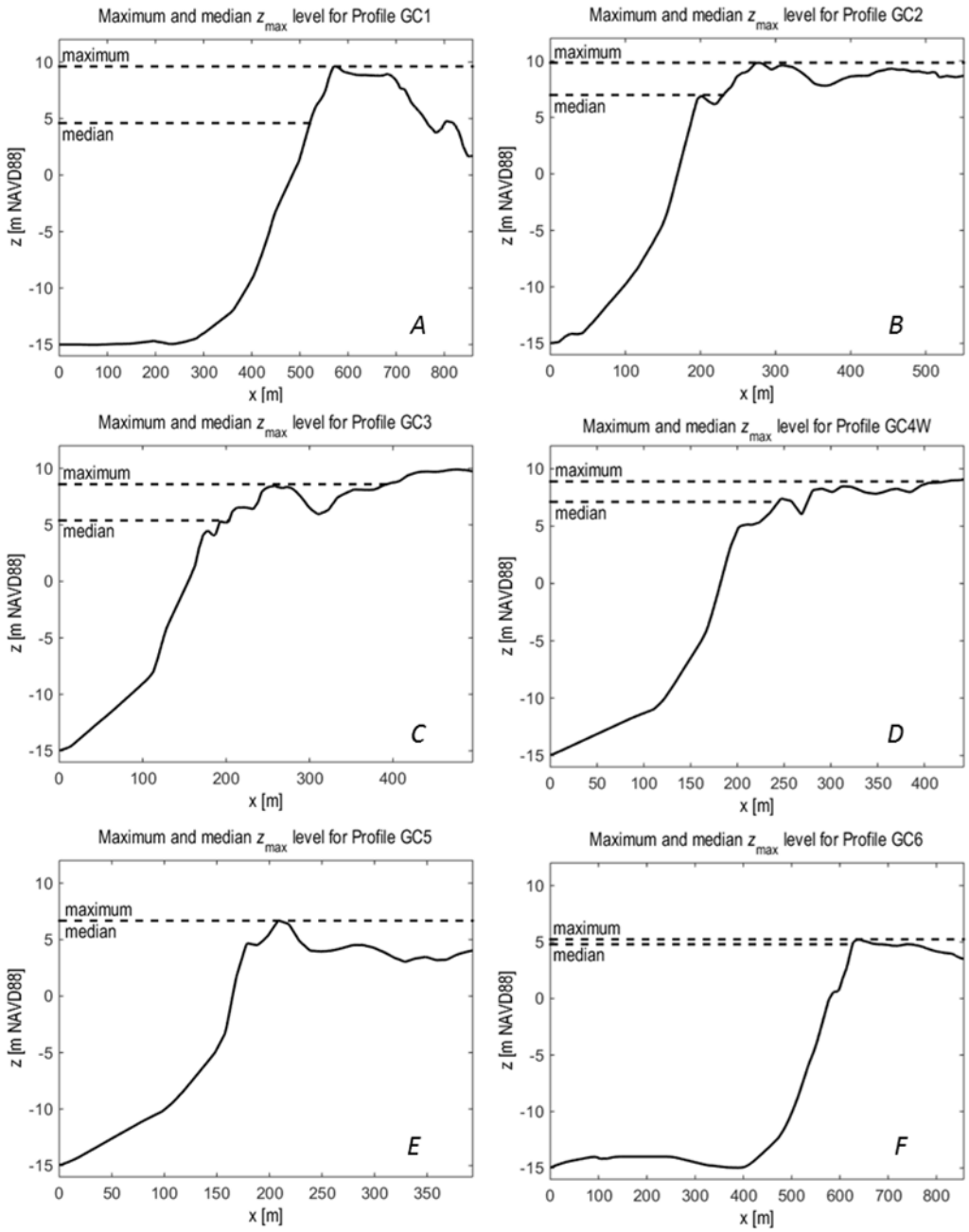


Figure 17. Graphs showing maximum and median water levels (storm surge+wave runup, $z_{max}$) of 30 storms simulated between 1985 and 2012 at Gambell, Alaska. *A–D*, Profiles GC1 through GC4 on the west coast of Gambell. *E–F*, Profiles GC5 and GC6 on the north coast of Gambell. Profile GC4 is located at Northwest Cape and is subject to both westerly and northerly storms. Maximum water levels at the crest of the profie are indicative of overtopping. Only results for the more severe westerly storms are shown here. Results do not include variations in water level due to tides. Note the difference in vertical scale between the west and north coast elevations. m, meters; NAVD88, North American Vertical Datum of 1988.

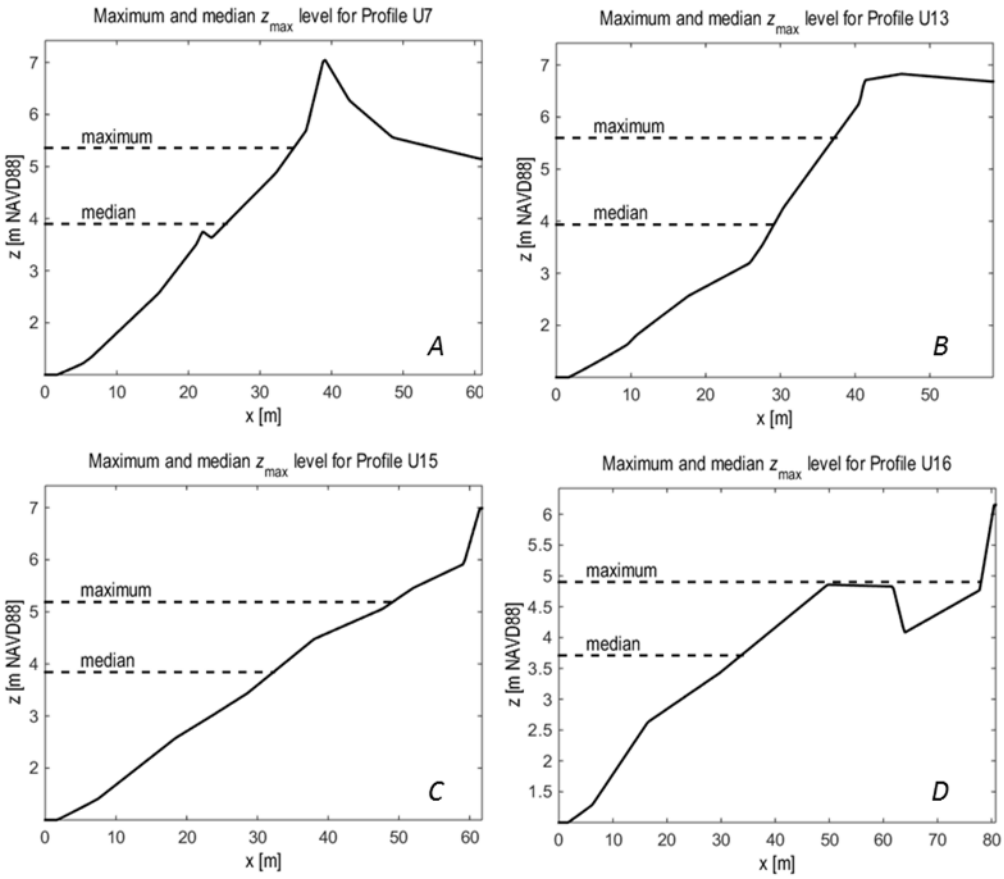


Figure 18. Graphs showing maximum and median water levels (storm surge+wave runup, $z_{max}$) of 30 storms simulated between 1985 and 2012 at Unalakleet, Alaska. *A*, Profile U7 located about 4 kilometers north of Unalakleet. *B–D*, Profiles U13, U15, and U16 along the open coast of Unalakleet. Results do not include variations in water level due to tides. m, meters; NAVD88, North American Vertical Datum of 1988.

Model simulations ranked the November 1996 storm as the highest $z_{max}$ at Gambell for the 1985–2012 time period. Overtopping of beach berm crests was estimated to have occurred at four of the six transects (GC1, GC2, GC5, and GC6) for this event. Although the north coast of Gambell experiences lower runup heights, the lower relief along transects GC5 and GC6 allowed overtopping and flooding to occur during 8 to 18 of the 30 storms simulated.

Wave conditions offshore of Unalakleet were hindcast to be much smaller and in most cases shorter (lower $T_p$) compared to Gambell (table 10). Because Norton Sound, the body of water immediately fronting Unalakleet, is shallow (generally less than 8 m in depth), wave growth is limited, and the energy of longer swell waves is reduced through refraction and dissipation. Although it is expected that wave heights and runup would be lower at Unalakleet compared to Gambell, it appears that modeled wave runups at Unalakleet are underestimated (see previous section).

Table 10. Wave conditions at the 15-meter isobath and consequent wave runup plus storm surge (relative to North American Vertical Datum of 1988, NAVD88) at the shore for the strongest 30 storms at Gambell, Alaska, between 1985 and 2012, transects GC2 and GC6.

[SWH, significant wave heights; $T_p$, peak period; $D_p$, peak direction; $z_{max,}$ storm surge+wave runup; s, second; m, meter; N, north; S, south; W, west]

| Transect GC2: Western exposure | | | | | | Transect GC6: Northern exposure | | | | | |
|---|---|---|---|---|---|---|---|---|---|---|---|
| Storm date | max SWH (m) | $T_p$ (s) | $D_p$ (deg. and compass description) | | $z_{max}$ (m) | Storm date | max SWH (m) | $T_p$ (s) | $D_p$ (deg. and compass description) | | $z_{max}$ (m) |
| Oct. 28, 1996 | 6.4 | 14 | 245 | WSW | 9.2 | Oct. 28, 1996 | 6.7 | 14 | 235 | SW | 5.3 |
| Nov. 9, 2011 | 6.0 | 12 | 245 | WSW | 9.0 | Nov. 9, 2011 | 6.2 | 12 | 235 | SW | 5.0 |
| Oct. 20, 2004 | 6.0 | 12 | 245 | WSW | 9.0 | Oct. 20, 2004 | 6.2 | 12 | 235 | SW | 4.5 |
| Oct. 27, 2010 | 3.5 | 14 | 245 | WSW | 8.1 | Oct. 10, 1989 | 4.1 | 9 | 245 | WSW | 4.4 |
| Nov. 12, 1992 | 2.9 | 12 | 245 | WSW | 6.3 | Nov. 4, 2000 | 2.9 | 9 | 335 | NNW | 4.4 |
| Nov. 1, 1997 | 2.7 | 9 | 225 | SW | 6.2 | Nov. 3, 2011 | 2.8 | 9 | 335 | NNW | 4.4 |
| Nov. 5, 1994 | 2.9 | 12 | 245 | WSW | 6.2 | Oct. 26, 2004 | 2.7 | 9 | 345 | NNW | 4.4 |
| Dec. 3, 2006 | 2.8 | 9 | 245 | WSW | 6.2 | Oct. 27, 2010 | 3.7 | 14 | 235 | SW | 4.4 |
| Oct. 15, 2004 | 2.9 | 9 | 235 | SW | 6.2 | Nov. 13, 2000 | 2.5 | 8 | 345 | NNW | 4.4 |
| Nov. 26, 1993 | 2.8 | 9 | 275 | W | 6.2 | Nov. 3, 1996 | 3.4 | 11 | 345 | NNW | 4.4 |
| Nov. 9, 2000 | 2.5 | 12 | 245 | WSW | 6.2 | Nov. 26, 2006 | 1.9 | 9 | 345 | NNW | 4.4 |
| Nov. 20, 1997 | 2.8 | 12 | 245 | WSW | 6.1 | Nov. 22, 2004 | 2.4 | 9 | 225 | SW | 4.2 |
| Oct. 5, 1992 | 2.6 | 8 | 245 | WSW | 6.1 | Nov. 15, 1989 | 2.2 | 11 | 225 | SW | 4.2 |
| Oct. 10, 1989 | 3.6 | 9 | 245 | WSW | 6.1 | Nov. 18, 2011 | 1.6 | 8 | 345 | NNW | 4.0 |
| Dec. 6, 2007 | 1.8 | 12 | 235 | SW | 6.1 | Nov. 12, 1992 | 3.0 | 12 | 235 | SW | 3.9 |
| Oct. 12, 2000 | 2.6 | 9 | 235 | SW | 6.1 | Oct. 30, 1995 | 1.6 | 9 | 345 | NNW | 3.9 |
| Nov. 3, 1996 | 2.8 | 11 | 235 | SW | 6.1 | Nov. 9, 1985 | 1.7 | 9 | 225 | SW | 3.9 |
| Oct. 30, 2003 | 2.4 | 11 | 235 | SW | 6.1 | Nov. 14, 1997 | 2.1 | 7 | 245 | WSW | 3.7 |
| Nov. 4, 2000 | 1.7 | 9 | 325 | NW | 6.1 | Nov. 1, 1997 | 2.9 | 9 | 225 | SW | 3.7 |
| Nov. 15, 1989 | 1.8 | 11 | 225 | SW | 6.1 | Oct. 26, 1991 | 1.8 | 8 | 345 | NNW | 3.6 |
| Sep. 13, 2010 | 2.0 | 9 | 225 | SW | 6.1 | Nov. 20, 1997 | 2.9 | 12 | 235 | SW | 3.4 |
| Nov. 22, 2004 | 2.3 | 9 | 225 | SW | 5.9 | Nov. 26, 1993 | 3.0 | 9 | 275 | W | 3.3 |
| Oct. 12, 1993 | 1.4 | 14 | 245 | WSW | 5.9 | Nov. 9, 2000 | 2.6 | 12 | 235 | SW | 3.3 |
| Nov. 9, 1985 | 1.6 | 9 | 225 | SW | 5.8 | Oct. 30, 2003 | 2.5 | 11 | 235 | SW | 3.2 |
| Nov. 9, 1993 | 2.0 | 11 | 235 | SW | 5.7 | Nov. 15, 1987 | 2.2 | 8 | 335 | NNW | 2.7 |
| Nov. 11, 1998 | 2.0 | 12 | 245 | WSW | 5.7 | Nov. 4, 1985 | 2.3 | 8 | 345 | NNW | 2.7 |
| Apr. 13, 1989 | 1.9 | 9 | 235 | SW | 5.6 | Oct. 9, 2008 | 2.2 | 7 | 335 | NNW | 2.6 |
| Nov. 3, 2011 | 1.8 | 9 | 325 | NW | 5.6 | Nov. 11, 1998 | 2.1 | 12 | 235 | SW | 2.5 |
| Oct. 16, 1987 | 3.2 | 8 | 245 | WSW | 5.3 | Oct. 20, 1986 | 2.6 | 8 | 345 | NNW | 2.4 |
| Oct. 13, 2008 | 1.8 | 11 | 245 | WSW | 5.1 | Aug. 19, 1998 | 2.3 | 8 | 275 | W | 2.0 |

Table 11. Wave conditions at the 8-meter isobath and consequent wave runup plus storm surge (relative to North American Vertical Datum of 1988, NAVD88) at the shore for the strongest 30 storms at Unalakleet, Alaska, between 1985 and 2012, transects U7 and U16.

[SWH, significant wave heights; $T_p$, peak period; $D_p$, peak direction; $z_{max,}$ storm surge+wave runup; s, second; m, meter; N, north; S, south; E, east; W, west]

| Transect U7 | | | | | | Transect U16 | | | | | |
|---|---|---|---|---|---|---|---|---|---|---|---|
| Storm date | max SWH (m) | $T_p$ (s) | $D_p$ (deg. and compass description) | | $z_{max}$ (m) | Storm date | max SWH (m) | $T_p$ (s) | $D_p$ (deg. and compass description) | | $z_{max}$ (m) |
| Oct. 19, 2004 | 0.9 | 4 | 225 | SW | 3.9 | Oct. 19, 2004 | 0.7 | 4 | 235 | SW | 3.5 |
| Sep. 6, 1990 | 1.0 | 5 | 235 | SW | 3.5 | Oct. 28, 2006 | 0.8 | 18 | 255 | WSW | 3.3 |
| Nov. 9, 2003 | 1.0 | 6 | 235 | SW | 3.3 | Sep. 06, 1990 | 0.8 | 5 | 245 | WSW | 3.3 |
| Aug. 27, 1990 | 1.0 | 5 | 235 | SW | 3.2 | Oct. 28, 1996 | 0.7 | 12 | 255 | WSW | 3.1 |
| Oct. 28, 1996 | 1.0 | 12 | 255 | WSW | 3.1 | Nov. 9, 2003 | 0.8 | 6 | 245 | WSW | 3.0 |
| Nov. 12, 2009 | 1.0 | 6 | 235 | SW | 3.1 | Aug. 27, 1990 | 0.8 | 4 | 245 | WSW | 2.9 |
| Oct. 15, 2004 | 0.9 | 18 | 255 | WSW | 3.0 | Nov. 12, 2009 | 0.8 | 5 | 245 | WSW | 2.8 |
| Aug. 25, 2012 | 0.9 | 4 | 235 | SW | 2.9 | May. 19, 1997 | 0.7 | 16 | 255 | WSW | 2.7 |
| Oct. 22, 1991 | 0.8 | 5 | 245 | WSW | 2.9 | Aug. 25, 2012 | 0.7 | 4 | 245 | WSW | 2.7 |
| Oct. 4, 1997 | 0.9 | 5 | 245 | WSW | 2.8 | Oct. 22, 1991 | 0.7 | 4 | 245 | WSW | 2.6 |
| Sep. 23, 2005 | 0.9 | 4 | 205 | SSW | 2.7 | Oct. 15, 2004 | 0.7 | 18 | 255 | WSW | 2.6 |
| Sep. 2, 2000 | 0.9 | 4 | 225 | SW | 2.7 | Sep. 2, 2000 | 0.7 | 4 | 245 | WSW | 2.4 |
| Oct. 2, 1993 | 1.0 | 4 | 215 | SW | 2.6 | Oct. 4, 1997 | 0.8 | 5 | 255 | WSW | 2.4 |
| Nov. 22, 2003 | 0.9 | 5 | 245 | WSW | 2.5 | Oct. 2, 1993 | 0.8 | 4 | 235 | SW | 2.3 |
| Oct. 28, 2006 | 1.0 | 18 | 255 | WSW | 2.5 | Nov. 22, 2003 | 0.8 | 4 | 255 | WSW | 2.3 |
| Nov. 10, 2011 | 0.9 | 4 | 235 | SW | 2.5 | Sep. 23, 2005 | 0.7 | 3 | 225 | SW | 2.3 |
| Sep. 1, 2009 | 0.8 | 4 | 215 | SW | 2.4 | Nov. 10, 2011 | 0.7 | 4 | 245 | WSW | 2.2 |
| Oct. 19, 1989 | 0.9 | 4 | 235 | SW | 2.4 | Aug. 15, 1988 | 0.6 | 4 | 235 | SW | 2.2 |
| Aug. 15, 1988 | 0.8 | 4 | 215 | SW | 2.4 | Jul. 20, 1986 | 0.6 | 4 | 245 | WSW | 2.2 |
| Jul. 20, 1986 | 0.8 | 4 | 235 | SW | 2.4 | Sep. 01, 2009 | 0.6 | 4 | 235 | SW | 2.2 |
| Aug. 2, 1996 | 0.9 | 4 | 235 | SW | 2.4 | Oct. 19, 1989 | 0.7 | 4 | 245 | WSW | 2.2 |
| Oct. 6, 1992 | 0.7 | 3 | 195 | SSW | 2.4 | Sep. 3, 1995 | 0.8 | 4 | 255 | WSW | 2.1 |
| Sep. 3, 1995 | 0.9 | 5 | 235 | SW | 2.4 | Aug. 2, 1996 | 0.7 | 4 | 245 | WSW | 2.1 |
| May. 19, 1997 | 1.0 | 16 | 255 | WSW | 2.4 | Nov. 15, 1996 | 0.5 | 2 | 125 | SE | 2.1 |
| Oct. 9, 2007 | 0.7 | 4 | 235 | SW | 2.3 | Oct. 6, 1992 | 0.6 | 3 | 135 | SE | 2.0 |
| Sep. 26, 1999 | 0.7 | 4 | 235 | SW | 2.3 | Oct. 9, 2007 | 0.6 | 4 | 235 | SW | 2.0 |
| Nov. 15, 1996 | 0.6 | 3 | 125 | SE | 2.2 | Sep. 26, 1999 | 0.6 | 4 | 245 | WSW | 1.9 |
| Nov. 3, 1990 | 0.7 | 4 | 235 | SW | 2.2 | Aug. 4, 1997 | 0.4 | 2 | 135 | SE | 1.9 |
| Aug. 4, 1997 | 0.5 | 3 | 195 | SSW | 2.1 | Nov. 3, 1990 | 0.5 | 4 | 245 | WSW | 1.9 |
| Dec. 2, 2006 | 0.8 | 4 | 235 | SW | 1.8 | Dec. 2, 2006 | 0.6 | 4 | 245 | WSW | 1.7 |

## Relative Contributions of Storm Surge, Wave Runup, and Tides

The variation in magnitude of storm surge and wave-runup elevations at Gambell and Unalakleet warrant further investigation into the relative contributions of individual processes on the TWL. Relative contributions were evaluated by combining results of the 30 XBeach storm runs with tide-generated water levels, separating each component and estimating the percent contributions from each. Tide levels were estimated with NOAA published tidal constituents for Savoonga and Unalakleet ($M_2$, $K_1$, $O_1$, $S_2$, $N_2$, $P_1$) and t-tide (Pawlowicz, 2006) for coincident timing with maximum storm-surge

elevations. Tides are about twice as large at Unalakleet as compared to Gambell/Savoonga and contribute 19 and 5 percent to the storm-related TWL at Unalakleet and Gambell, respectively. On the basis of the deterministic tide and storm-related water levels estimated herein, extreme TWLs are dominated by wave runup at Gambell and by storm surges at Unalakleet (fig. 19). It is estimated that 84 percent of the extreme TWL is derived from wave runup in Gambell (profile GC2), whereas in Unalakleet (profile U16), only 19 percent of the TWL is due to wave runup. The majority of the storm-related TWL at Unalakleet appears to be related to storm surge, representing more than 60 percent of the TWL. In an effort to account for the underestimated wave heights, one can assume a doubling of the runup. Even with this increase, storm surges remain the major component of TWLs at Unalakleet—surge at 53 percent, runup at 31 percent, and tides at 16 percent (fig. 19).

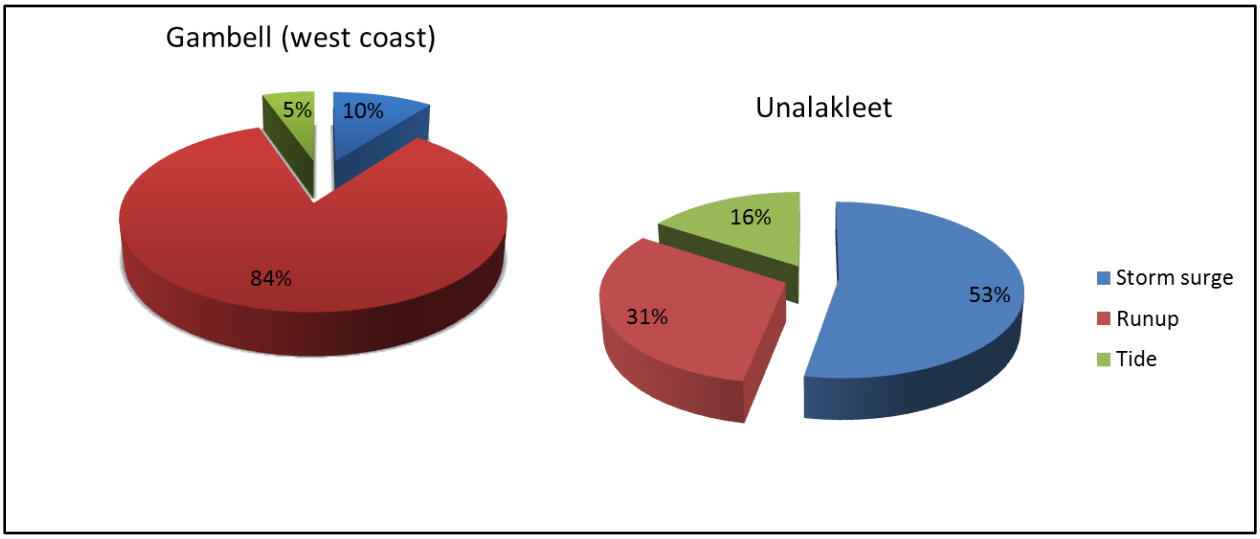


Figure 19. Pie diagrams showing relative contributions of storm surge, wave runup, and tides on total water levels at Gambell and Unalakleet, Alaska. Modeled values at profiles GC2 and U16 were employed in the calculations. Unalakleet values include a runup height twice what was modeled in an effort to correct for the undervalued boundary conditions of the wave model (see text for further explanations).

## Storm Frequency Analysis

Storm and stage frequency analysis were calculated and are tabulated for the 5-, 10-, 15-, 20-, 25-, 50-, and 100-year return periods (RPs; that is, water-level maxima at which there is a 20-, 10-, 7-, 5-, 4-, 2-, and 1-percent chance of occurrence per year). Return values were calculated using three common distributions to estimate extreme value statistic—generalized Pareto distribution (GPD), generalized extreme value (GEV), and log linear (LL). For details on these methods, the reader is referred to statistical textbooks such as Coles (2001).

Separate computations were made for the identified storm surges and $z_{max}$ (storm surge+runup). The strongest 32 (from 1981 through 2012) and 28 (from 1985 through 2012) storm events identified within each time-series were used for the storm-surge and $z_{max}$ extreme-value computations, respectively; this was done to represent an average of one storm per year. Results are summarized below.

## Storm Surges

Return-value curves fit to simulated storm-surge data at Gambell, Savoonga, and Unalakleet suggest that of the three sites studied Savoonga experiences the lowest storm-surge levels and Unalakleet experiences the highest, with levels that are typically ~1 m higher. Return values averaged over the three methods and used to estimate extreme statistics indicate that 5- to 100-year storm-surge levels range from 1.08±0.02 to 2.15±0.23 m MSL at Savoonga and 1.09±0.03 to 2.52±0.52 m MSL at Gambell (table 11 and fig. 20). At Unalakleet, the 5- to 100-year levels range from 2.19±0.02 to 3.44±0.19 m MSL.

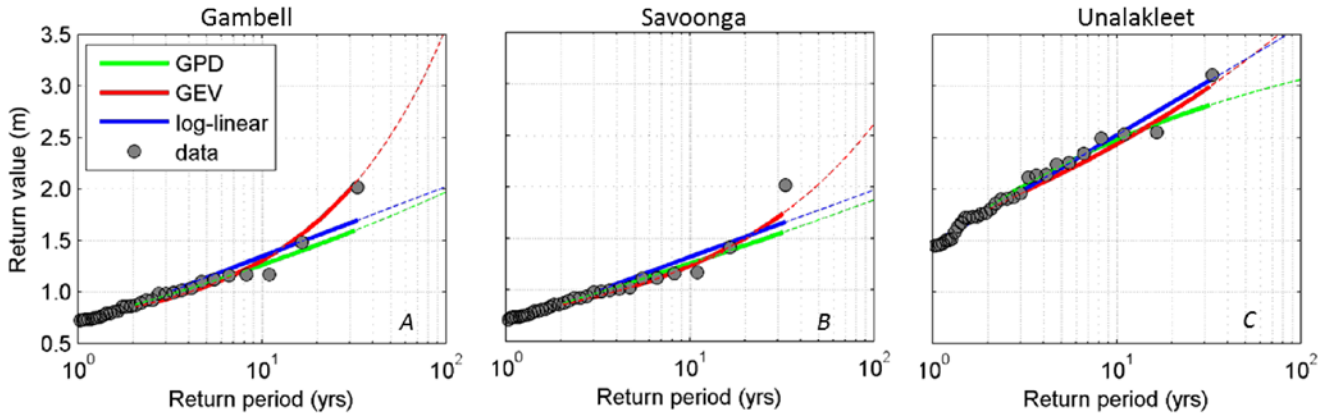


Figure 20. Extreme-value estimates using generalized Pareto distribution (GPD), generalized extreme value (GEV), and log-linear (LL) fits to storm-surge data at Gambell, Savoonga, and Unalakleet, Alaska. m, meters; yrs, years.

Table 12. Storm surge stage-frequency analysis for Gambell, Savoonga, and Unalakleet (in meters above mean sea level) using three methods of extreme value analysis.
[RP, return period, in years; GPD, generalized Pareto distribution; GEV, generalized extreme value; LL, log linear]

| RP | Gambell | | | | Savoonga | | | | Unalakleet | | | |
|---|---|---|---|---|---|---|---|---|---|---|---|---|
| | GPD | GEV | LL | Mean[1] | GPD | GEV | LL | Mean[1] | GPD | GEV | LL | Mean[1] |
| 5 | 1.08 | 1.06 | 1.14 | 1.09±0.03 | 1.08 | 1.04 | 1.12 | 1.08±0.02 | 2.23 | 2.15 | 2.21 | 2.19±0.02 |
| 10 | 1.26 | 1.30 | 1.35 | 1.30±0.02 | 1.25 | 1.23 | 1.32 | 1.27±0.03 | 2.48 | 2.43 | 2.52 | 2.48±0.03 |
| 15 | 1.37 | 1.51 | 1.46 | 1.45±0.04 | 1.36 | 1.38 | 1.43 | 1.39±0.02 | 2.60 | 2.61 | 2.71 | 2.64±0.03 |
| 20 | 1.46 | 1.68 | 1.55 | 1.56±0.07 | 1.43 | 1.50 | 1.52 | 1.48±0.03 | 2.69 | 2.75 | 2.84 | 2.76±0.04 |
| 25 | 1.52 | 1.84 | 1.61 | 1.66±0.10 | 1.49 | 1.61 | 1.58 | 1.56±0.04 | 2.75 | 2.86 | 2.94 | 2.85±0.06 |
| 50 | 1.74 | 2.52 | 1.82 | 2.02±0.25 | 1.68 | 2.02 | 1.77 | 1.83±0.10 | 2.92 | 3.24 | 3.26 | 3.14±0.11 |
| 100 | 1.97 | 3.56 | 2.02 | 2.52±0.52 | 1.87 | 2.61 | 1.97 | 2.15±0.23 | 3.06 | 3.68 | 3.58 | 3.44±0.19 |

[1]Uncertainty associated with the mean is the standard deviation of the mean, $SDOM = \sigma_m/\sqrt{N}$ where $\sigma_m$ is the standard deviation of the samples and $N$=3.

The three fitted curves agree well up to the 20- and 30-year return periods, but for the extrapolated data (dashed lines in fig. 20) the models deviate from one another. At Gambell and Savoonga, the GEV deviates substantially from the GPD and log-linear fits but better represents the

extreme value modeled at both sites. At Unalakleet, the scatter is somewhat lower, but here the GPD underestimates the return values at the extremes. Although it is tempting to assign a particular model to the data, it is recommended here that the average of the results be considered as the better representation of extreme events.

## Storm Surge Plus Wave Runup

Return value curves fit to simulated data for storm surge plus wave runup at Gambell and Unalakleet suggest that $z_{max}$ is much larger at Gambell compared to Unalakleet. Tables 13 and 14 list the average values of GPD, GEV, and LL extreme-value fits for each of the cross-shore profiles at Gambell and Unalakleet, respectively. The profiles on the west shores of Gambell exhibit higher $z_{max}$ compared to the north shore. The maximum 100-year return level is estimated to be 9.83±0.16 m MSL at GC2 compared to the maximum on the north coast, which is estimated to be 7.63±0.08 m MSL at GC5. Profile GC4, located near the northwest point and exposed to waves from both the west and north, experiences $z_{max}$ levels that are on average 30 percent higher when subjected to westerly compared to northerly storms (compare $z_{max}$ results of GC4W and GC4N in table 13). Interestingly, the difference between the 5- and 100-year return period levels are smaller at profiles GC4 through GC6 compared to the west exposed profiles GC1 through GC3 (fig. 21*A*). This is likely a response to the shallows north of Gambell, which provide a mode for waves of varying height and period to dissipate energy as they traverse across the rather shallow bathymetry. The deeper waters along the west coast allow larger waves to reach the shores before "feeling" the bottom and dissipating energy.

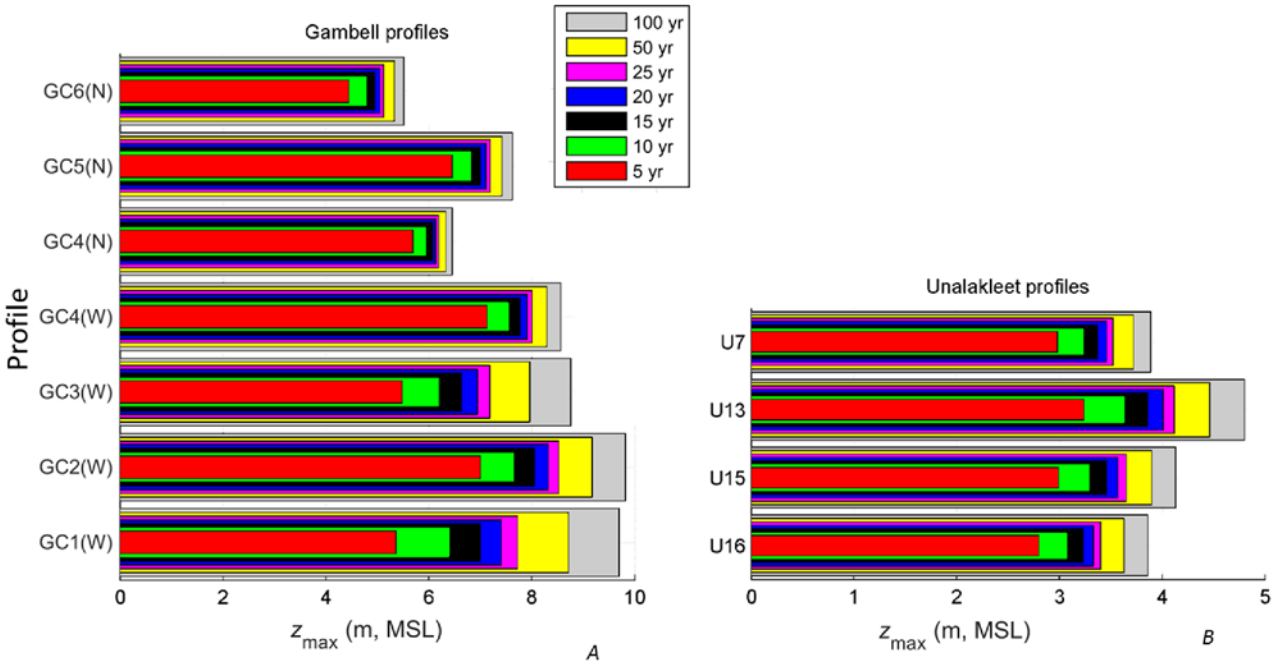


Figure 21. Diagrams showing storm surge plus wave runup ($z_{max}$) levels for select return periods and profiles at Gambell and Unalakleet, Alaska. *A*, Profiles along the west (GC1 through GC4) and north shores (GC4 to GC6) of Gambell. *B*, Profiles from north (U7) to south in the vicinity of Unalakleet. At Unalakleet, $z_{max}$ values are likely too low due to an underestimate of runup by ~1.5 meters (see text). N, north; W, west; m, MSL, meters relative to mean sea level; yr, year.

At Unalakleet, $z_{max}$ is expected to be highest at profile U13 at the north end of the community with an estimated highest 100-year $z_{max}$ 4.80±0.32 m for all return periods (table 14 and fig. 21*B*). This can partly be attributed to the milder foreshore slope (beach gradient, tan$\beta$=0.06) compared to the slope at U7 (tan$\beta$=0.10), where the waves are slightly larger due to the lack of an alongshore bar or shoal.

Table 13. Storm surge plus wave runup stage-frequency analysis for Gambell, Alaska, transects, in meters above mean sea level (mean of generalized Pareto distribution, generalized extreme value, and log linear fits).
[RP, return period, in years]

| RP | GC1 | GC2 | GC3 | GC4W | GC4N | GC5 | GC6 |
|---|---|---|---|---|---|---|---|
| 5 | 5.37±0.20 | 7.00±0.12 | 5.49±0.07 | 7.13±0.20 | 5.69±0.25 | 6.45±0.17 | 4.45±0.17 |
| 10 | 6.41±0.24 | 7.67±0.15 | 6.21±0.07 | 7.56±0.12 | 5.95±0.30 | 6.83±0.13 | 4.80±0.13 |
| 15 | 7.00±0.23 | 8.05±0.16 | 6.64±0.05 | 7.77±0.06 | 6.07±0.32 | 7.01±0.09 | 4.95±0.09 |
| 20 | 7.41±0.20 | 8.32±0.15 | 6.95±0.03 | 7.91±0.07 | 6.14±0.33 | 7.19±0.06 | 5.05±0.06 |
| 25 | 7.73±0.18 | 8.53±0.15 | 7.19±0.03 | 8.01±0.10 | 6.19±0.33 | 7.20±0.05 | 5.13±0.05 |
| 50 | 8.71±0.09 | 9.18±0.12 | 7.96±0.12 | 8.29±0.25 | 6.33±0.34 | 7.43±0.15 | 5.33±0.12 |
| 100 | 9.70±0.21 | 9.83±0.16 | 8.76±0.29 | 8.56±0.42 | 6.45±0.35 | 7.63±0.28 | 5.52±0.24 |

Table 14. Storm surge plus wave runup stage-frequency analysis for Unalakleet, Alaska, transects, in meters above mean sea level (mean of generalized Pareto distribution, generalized extreme value, and log linear fits).
[RP, return period, in years]

| RP | U16 | U15 | U13 | U7 |
|---|---|---|---|---|
| 5 | 2.80±0.07 | 2.99±0.07 | 3.24±0.10 | 2.98±0.09 |
| 10 | 3.08±0.04 | 3.30±0.05 | 3.64±0.05 | 3.24±0.11 |
| 15 | 3.23±0.02 | 3.46±0.03 | 3.86±0.02 | 3.37±0.11 |
| 20 | 3.33±0.02 | 3.57±0.03 | 4.01±0.04 | 3.46±0.11 |
| 25 | 3.40±0.04 | 3.65±0.05 | 4.12±0.07 | 3.52±0.10 |
| 50 | 3.63±0.11 | 3.90±0.12 | 4.46±0.19 | 3.72±0.08 |
| 100 | 3.86±0.20 | 4.13±0.22 | 4.80±0.32 | 3.89±0.06 |

## Discussion and Conclusion

Continuous time-series of changes in water levels during the open-water seasons from 1981 through 2012 were simulated for the Bering Sea region using a numerical model and spatially and time-varying wind fields. From the time-series, discrete storm events were identified and used to estimate extreme value curves extending out to the 100-year return period at Gambell and Savoonga on St. Lawrence Island and at Unalakleet, located on the mainland shore of western Alaska.

Maximum storm-surge levels calculated for the 1981–2012 time period reached 2.02 m MSL at the western and northern exposed coasts of Gambell and Savoonga and 3.10 m at Unalakleet. Unalakleet experienced the highest storm-surge levels followed by Gambell and Savoonga. Simulation results did not show any appreciable difference between storm-surge elevations on the west and north sides of Gambell and only show small differences between Gambell and Savoonga. The number of annual extreme storm-surge events, counted as those that exceeded the 90th percentile of the 1981–2012 time period, were at most seven but often occurred five or six times during any given year. Although

there is a statistically significant trend of 0.5 days per year for the return of the pack ice in the fall season, model results did not show any clear trend of increasing storm-surge height or frequency with respect to time as might be expected with increased open-water duration and typical storm occurrence late in the year. This result potentially indicates that storm intensity and frequency are not substantially greater later in the fall season or that the time of record may not be long enough to observe a strong signal of increased intensity or frequency.

Extreme value analyses indicate that 5- to 100-year storm-surge levels range from 1.09±0.03 m to 2.52±0.52 m MSL at Gambell and from 2.19±0.02 to 3.44±0.19 m MSL at Unalakleet. The extrapolated return period values are based on the hindcast results encompassing 32 years and assume a stationary climate.

The impact of wave runup in addition to storm surge on the total water level and flooding potential was evaluated along specific profiles on the Gambell and Unalakleet coasts. The analysis was performed for the time period between 1985 and 2012, somewhat shorter compared to the storm-surge computations, with the beginning date representing the year in which hindcast offshore wave data were available. In cases of the same storm event, the combined contribution of storm surge and wave runup ($z_{max}$) was greater on the western exposed coast of Gambell compared to the north coast, and in some cases it was more than twice as high. This is likely related to the shoal on the north of side Gambell across which waves more readily dissipate energy as they refract and break further from the coast resulting in overall lower runup heights compared to the west side. This was particularly evident along profile GC4, located at the northwest point of Gambell and subject to both westerly and northerly storms.

In Gambell, the maximum hindcast $z_{max}$ levels were estimated to have reached 9.2 and 5.3 m MSL (October 1996) on the west and north coasts (profiles GC2 and GC6), respectively. Based on extreme value computations, these levels correspond to an approximate 50-year event. The 100-year events are projected to be slightly higher at 9.83±0.16 and 5.52±0.24 m MSL for profiles GC2 and GC6, respectively.

Unalakleet $z_{max}$ levels (October 2004) were hindcast to have reached 3.9 m MSL at profiles U7, located ~5 km north of the community, and 3.5 m MSL at profile U16 at the south end of the community. The November 2011 storm was ranked as the 16th to 17th most powerful amongst the 30 storms simulated for the 1985–2012 time period but appears to be underestimated with respect to field observations documented by Kinsman and DeRaps (2012). A discrepancy of more than 1 m between observed and calculated $z_{max}$ levels for the November 2011 storm combined with low wave heights throughout Norton Sound has led us to suspect that the wave-runup heights calculated as part of this study are underestimated at Unalakleet. A substantial alongshore bar immediately offshore of the community mitigates some of the wave energy approaching the shore but does not fully explain the low runup heights attained for the 30 storms simulated between 1985 and 2012 (max runup=1.7 m above still water, profile U7 ~5 km north of Unalakleet). Wave-boundary forcings employed in this study were obtained from the WIS hindcast database, but compared to an independent global wave reanalysis product (ERA Interim), SWHs are severely biased low ( about half of ERA-I SWHs), likely explaining the low runup heights calculated for Unalakleet. In contrast, there is good agreement between ERA-I and WIS wave conditions used as boundary forcing in the Gambell wave model, and thus the confidence in the wave runup estimates for Gambell is high.

Relative contributions of storm surge, wave runup, and tides on the total water level were evaluated for both Gambell and Unalakleet. For this evaluation, runup heights modeled at Unalakleet were doubled to roughly account for the suspected undervalued SWHs used as open-boundary conditions in the model. Relative contributions were evaluated by combining results of individual water

level components with deterministically derived tide levels, separating each component and estimating the percent contributions from each. Results show that tides are about twice as large at Unalakleet compared to Gambell and contribute 16 and 5 percent to the storm-related TWL at Unalakleet and Gambell, respectively. Storm-related TWLs are dominated by wave runup (84 percent) at Gambell and by storm surges (more than 53 percent ) at Unalakleet. Surge levels and tides are accentuated at Unalakleet because of the semi-enclosed basin (Norton Sound) and shallow water depths; the same shallow water depths limit local wave growth and reduce longer wave energy through refraction and dissipation, thus reducing the relative contribution of wave runup on TWL. In contrast, Gambell's location in the near center of the Bering Sea allows for rapid return flows of storm surge and exposure to large waves capable of significant wave runup.

## References Cited


Andreas, E.L., Lange, M.A., Ackley, S.F., and Wadhams, P., 1993, Roughness of Weddell Sea ice and estimates of the air–ice drag coefficient: Journal of Geophysical Research, v. 98, no. C7, p. 12439–12452.

Battjes, J., and Janssen, J., 1978, Energy loss and set-up due to breaking of random waves: American Society of Civil Engineers, Proceedings 16th International Conference Coastal Engineering, p. 569–587.

Birnbaum, G., and Lupkes, C., 2002, A new parameterization of surface drag in the marginal sea ice zone: Tellus, v. 74, p. 107–23.

Booij, N., Ris, R.C., and Holthuijsen, L.H., 1999, A third-generation wave model for coastal regions—Model description and validation: Journal of Geophysical Research, v. 104, no. C4, p. 7649–7666.

Bouws, E., and Komen, G.J., 1983, On the balance between growth and dissipation in an extreme, depth-limited wind-sea in the southern North Sea: Journal of Physical Oceanography, v. 13, p. 1653−1658.

Broström, G., and Christensen, K., 2008, Waves in sea ice: Norwegian Meteorological Institute, report no. 5/2008, 63 p.

Chapman, R.S., Kim, S-C., and Mark, D.J., 2009, Storm damage and flooding evaluation, storm induced water level prediction study for the western coast of Alaska: Vicksburg, Mississippi, U.S. Army Engineer Research and Development Center, Coastal and Hydraulics Laboratory (ERDC/CHL) Letter Report, 92 p.

Charnock, H., 1955, Wind stress on a water surface: Quarterly Journal of the Royal Meteorological Society, v. 81, p. 639–640.

Coles, S., 2001, An introduction to statistical modeling of extreme values: Springer, 70 p., doi:10.1007/978-1-4471-3675-0.

Cross, A.E., 2010, Synoptic drivers of storm surge in Kotzebue Sound: University of Alaska at Fairbanks, M.S. thesis, 94 p.

Danielson, S., Aagaard, K., Weingartner, T., Martin, S., Winsor, P., Gawarkiewicz, G., and Quadfasel D., 2006, The St. Lawrence polynya and the Bering shelf circulation—New observations and a model comparison: Journal of Geophysical Research, 111, C09023.

Danielson, S., and Kowalik, Z., 2005, Tidal currents in the St. Lawrence Island region: Journal of Geophysical Research, v. 110, C10004, doi:10.1029/2004JC002463.

Dee, D.P., Uppala, S.M., Simmons, A.J., Berrisford, P., Poli, P., Kobayashi, S., Andrae, U., Balmaseda, M.A., Balsamo, G., Bauer, P., Bechtold, P., Beljaars, A.C.M., van de Berg, L., Bidlot, J., Bormann, N., Delsol, C., Dragani, R., Fuentes, M., Geer, A.J., Haimberger, L., Healy, S. B., Hersbach, H.,

Hólm, E.V., Isaksen, L., Kållberg, P., Köhler, M., Matricardi, M., McNally, A.P., Monge-Sanz, B. M., Morcrette, J-J., Park, B-K., Peubey, C., de Rosnay, P., Tavolato, C., Thépaut, J-N., and Vitart, F., 2011, The ERA-Interim reanalysis—Configuration and performance of the data assimilation system: Quarterly Journal of the Royal Meteorological Society, v. 137, p. 553–597.

Deltares, 2011, Delft3D-FLOW—Simulation of multi-dimensional hydrodynamic flows and transport phenomena, including sediments—User manual, ver. 3.14, rev. 11214: Delft, Netherlands, Deltares, 672 p.

Döscher, R., Vihma, T., and Maksimovich, E., 2014, Recent advances in understanding the Arctic climate system state and changes from a sea ice perspective a review: Atmospheric Chemistry and Physics, v. 14, p. 13571–13600.

Earth System Research Laboratory, 2014, North American Regional Reanalysis (NARR) for Arctic Research: National Oceanic and Atmospheric Administration, Earth System Research Laboratory dataset, accessed March, 17, 2014, at http://www.esrl.noaa.gov/psd/data/gridded/data.narr.html.

Egbert, G., and Erofeeva, S., 2002, Efficient inverse modeling of barotropic ocean tides: Journal of Atmospheric and Oceanic Technology, v. 19, no. 2, p. 183–204.

Federal Aviation Administration (FAA), 2014, Airport Master Record for Gambell Airport: U.S. Department of Transportation, Form Approved OMB 2120-0015.

Garbrecht, T., Lupkes, C., Hartmann, J., and Wolff, M., 2002, Atmospheric drag coefficients over sea ice-validation of a parameterization concept: Tellus, v. 54A, p. 205–219.

Garratt, J., 1977, Review of drag coefficients over oceans and continents: Monthly Weather Review, v. 105, no. 7, p. 915–929.

General Bathymetric Chart of the Oceans (GEBCO), 2010, GEBCO 2008 grid: General Bathymetric Chart of the Oceans dataset, accessed April 2010 at http://www.gebco.net/data_and_products/gridded_bathymetry_data/.

Gunther, H., Hasselmann, S., and Janssen, P.A.E.M., 1992, WAM model cycle 4: Reading, England, European Center for Medium Range Weather Forecast, Technical Report No. 4, p. 102.

Hansen, K., 2014, Storm aimed for Aleutian Islands: National Aeronautics and Space Administration (NASA) Earth Observatory News Feed, accessed December 2014 at http://earthobservatory.nasa.gov/NaturalHazards/view.php?id=84695.

Hasselmann, K., Barnett, T.P., Bouws, E., Carlson, H., Cartwright, D.E., Enke, K.,. Ewing, J.A, Gienapp, H., Hasselmann, D.E., Kruseman, P., Meerburg, A., Müller, P., Olbers, D.J., Richter, K., Sell, W., and Walden, H., 1973, Measurements of wind-wave growth and swell decay during the Joint North Sea Wave Project (JONSWAP): Deutschen Hydrographischen Zeitschrift, v. 8, no. 12, suppl. A., p. 95.

Henry, R.F., and Heaps, N.S., 1976, Storm surge in the southern Beaufort Sea: Journal of the Fisheries Research Board of Canada, v. 33, no. 10, p. 2362–2376.

Hughes, C., 1984, Saint Lawrence Island Eskimo, *in* Damas, D., ed., Handbook of North American Indians, vol. 5—Arctic: Washington, D.C., Smithsonian Institution Press, p. 262–277.

Hume, J.D., and Schalk, M., 1967, Shoreline processes near Barrow, Alaska; a comparison of the normal and the catastrophic: Arctic, v. 20, p. 86–103.

Jensen, R., 2010, Wave Information Studies (WIS) project documentation: U.S. Army Corps of Engineers Web page, accessed June 1, 2014, at http://wis.usace.army.mil/WIS_Documentation.shtml [data available at http://wis.usace.army.mil/].

Johnson, W.R., and Kowalik, Z., 1986, Modeling of storm surges in the Bering Sea and Norton Sound: Journal of Geophysical Research, v. 91, p. 5119–5128.

Kinsman, N.E.M., 2015, Single-beam bathymetry data collected in shallow-water areas near Gambell, Golovin, Hooper Bay, Savoonga, Shishmaref, and Wales, Alaska, 2012–2013: Alaska Division of Geological and Geophysical Surveys Raw Data File 2015-2, 15 p., http://dx.doi.org/10.14509/29348.
Kinsman, N.E.M., and DeRaps, M.R., 2012, Coastal hazard field activities in response to the November 2011 Bering Sea storm, Norton Sound, Alaska: Alaska Division of Geological and Geophysical Surveys Report of Investigation 2012-2, ver. 1.1, 51 p.
Komen, G., Hasselmann, S, and Hasselmann, K., 1984, On the existence of a fully developed wind-sea spectrum: Journal of Physical Oceanography, v. 14, p. 1271–1285.
Komen, G.J, Cavaleri, L., Donelan, M., Hasselmann, K., Hasselmann, S., and Janssen, P.A.E.M., 1994, Dynamics and modeling of ocean waves: Cambridge University Press, 532 p.
Kowalik, Z., 1984, Storm surges in the Beaufort and Chukchi Seas: Journal of Geophysical Research, v. 89, no. 6, p. 10570–10578.
Lesser, G.R., Roelvink, J.A., van Kester, J.A.T.M., and Stelling, G.S., 2004, Development and validation of a three-dimensional morphological model: Coastal Engineering, v. 51, nos. 8–9, p. 883–915.
Lynch, A.H., Cassano, E.N., Cassano, J. J., and Lestak, L. R., 2003, Case studies of high wind events in Barrow, Alaska: Climatological context and development processes: American Meteorological Society, Monthly Weather Review, v. 131, p. 719–732.
Macklin, S.A., 1983. Wind drag coefficient over first-year sea ice in the Bering Sea: Journal of Geophysical Research, v. 88, no. C5, p. 2845–2852.
McCall, R.T., Masselink, G., Poate, T.G., Roelvink, J.A., Almeida, L.P., Davidson, M., and Russell, P.E., 2014, Modelling storm hydrodynamics on gravel beaches with XBEACH-G: Coastal Engineering, v. 91, p. 231–250.
Mesinger, F., DiMego, G., Kalnay, E., Mitchell, K., Shafran, P.C., Ebisuzaki, W., Jović, D., Woollen, J., Rogers, E., Berbery, E.H., Ek, M.B., Fan, Y., Grumbine, R., Higgins, W., Li, H., Lin, Y., Manikin, G., Parrish, D., and Shi, W., 2006, North American Regional Reanalysis: Bulletin of the American Meteorological Society, v. 87, no. 3, p. 343–360, http://dx.doi.org/10.1175/BAMS-87-3-343.
Mesquita, M.D., Atkinson, D.E., and Hodges, K.I., 2010, Characteristics and variability of storm tracks in the North Pacific, Bering Sea, and Alaska: Journal of Climate, v. 23, p. 294–311.
National Climatic Data Center (NCDC), 2014, Quality controlled local climatological data (QCLCD): National Oceanic and Atmospheric Administration, National Climatic Data Center Web page, accessed December 2014 at http://www.ncdc.noaa.gov/data-access/land-based-station-data/land-based-datasets/quality-controlled-local-climatological-data-qclcd.
National Geophysical Data Center, 2014, Bathymetry and Global Relief: National Oceanic and Atmospheric Administration, National Geophysical Data Center Web site, accessed April 2014 at http://www.ngdc.noaa.gov/mgg/batymetry/.
National Oceanic and Atmospheric Administration (NOAA), 2014, Tides and currents website. [http://tidesandcurrents.noaa.gov/, last accessed December 2014.
Oceanweather, Inc., 2006, Wind, pressure and ice concentration fields for Alaska long-term climatology: Contract report to U.S. Army Engineer Research and Development Center, Vicksburg, Miss.
Ostrom, J.E., Comiskey, A.L., and Miller, R.C., 1987, Atlas of Oceanographic Information for Norton Sound, Alaska: Springfield, Va., U.S. Coast Guard, Office of Engineering and Development.
Overland, J.E., and Pease, C.H., 1982, Cyclone climatology of the Bering Sea and its relation to sea ice extent: Monthly Weather Review, v. 110, p. 5–13.

Pawlowicz, R., Beardsley, B., and Lentz, S., 2002, Classical tidal harmonic analysis including error estimates in MATLAB using T-TIDE: Computers and Geosciences, v. 28, no. 8, p. 929–937.
Perovich, D.K., and Richter-Menge, J.A., 2009, Loss of sea ice in the Arctic: Annual Review of Marine Science, v. 1, p. 417–441.
Rodionov, S.N., Bond, N.A., and Overland, J.E., 2007, The Aleutian Low, storm tracks, and winter climate variability in the Bering Sea: Deep-Sea Research II, v. 54, p. 2560–2577.
Roelvink, D., Reniers, A., van Dongeren, A., van Thiel de Vries, J., McCall, R., and Lescinski, J., 2009, Modelling storm impacts on beaches, dunes and barrier islands: Coastal Engineering, v. 56, no. 11, p. 1133–1152.
Stopa, J.E., and Cheung, K.F., 2014, Intercomparison of wind and wave data from the ECMWF reanalysis interim and the NCEP climate forecast system reanalysis: Ocean Modelling, v. 75, p. 65–83.
Terenzi, J., Torre, J.M., and Ely, C.R., 2014, Storm surge flooding on the Yukon-Kuskokwim Delta, Alaska: Arctic, v. 67, no. 3, p. 360–374, http://dx.doi.org/10.14430/arctic4403.
U.S. Army Corps of Engineers, 2011, Civil Works and floodplain management services: U.S. Army Corps of Engineers, Alaska District  accessed March 17, 2014 XX, 2011, at http://206.174.16.211/floodplain_data/Unalakleet/Documents/.
U.S. Census Bureau, 2014, U.S. Census Bureau: U.S. Census Bureau Web site, accessed December 2014 at http://www.census.gov/.
Vatvani, D., Zweers, N.C., van Ormondt, M., Smale, A.J., de Vries, H., and Makin, V.K., 2012, Storm surge and wave simulations in the Gulf of Mexico using a consistent drag relation for atmospheric and storm surge models: Natural Hazards and Earth Systems Sciences, v. 12, p. 2399–2410,
Walsh, J.E., Overland, J.E., Groisman, P.Y., and Rudolf, B., 2011, On-going climate change in the Arctic: Ambio, v. 40, p. 6–16.
Walter, B.A., Jr., and Overland, J.E., 1984, Observations of longitudinal rolls in a near neutral atmosphere: Monthly Weather Review, v. 112, p. 200–208.
Willmott, C.J., 1981, On the validation of models: V.H. Winston and Sons, Physical Geography, v. 2, no. 2, p. 184–194.
Wise, J.L., Comiskey, A.L., and Becker, R.B., 1981, Storm surge climatology and forecasting in Alaska: University of Alaska, Arctic Environmental Information and Data Center, 32 p.

ISSN 2331-1258 (online)
http://dx.doi.org/10.3133/ofr20151193